



Cite this: *Energy Adv.*, 2023, 2, 574

## Review of the progress of solar-driven interfacial water evaporation (SIWE) toward a practical approach

Srishti, <sup>a</sup> Apurba Sinhamahapatra \*<sup>b</sup> and Aditya Kumar <sup>a</sup>

Solar-driven interfacial water evaporation (SIWE), which has shown a promising use in the fields of water evaporation, desalination, wastewater treatment, and other related activities, has emerged as a practical and effective method for capturing solar energy. SIWE device development and upgraded structural design with increased performance have received much attention in the last decade. In this review article, we revise the level of development achieved for different solar absorber materials and substrates, and their conceptual design in terms of light absorptivity, heat and water management, and structural engineering, along with various potential SIWE applications, including desalination, sterilization, wastewater evaporation, energy generation, and others. Finally, the progress regarding the recent advancements in scalable solar-driven clean water generation is presented. This review summarizes the inclusive development in SIWE from laboratory to practical applications, inspiring new thinking with solutions to the practical challenges and serving as an outline for future investigations.

Received 16th January 2023,  
Accepted 27th March 2023

DOI: 10.1039/d3ya00028a

rsc.li/energy-advances

<sup>a</sup> Department of Chemical Engineering, Indian Institute of Technology (ISM), Dhanbad, Dhanbad-826004, Jharkhand, India

<sup>b</sup> Water Resource Management, CSIR-Central Institute of Mining and Fuel Research (CSIR-CIMFR), Dhanbad-826015, Jharkhand, India.

E-mail: apurbasmp03@gmail.com, apurba@cimfr.nic.in



Srishti

*Mrs Srishti is currently a doctoral student at the Department of Chemical Engineering, Indian Institute of Technology (Indian School of Mines) in Dhanbad, Jharkhand. She completed a BTech (Bachelor of Technology) in Chemical Engineering from the BPUT-affiliated C.V. Raman College of Engineering in Odisha and an MTech (Master of Technology) in Chemical Engineering from B.I.T., Sindri, Jharkhand. She is working on the development of photothermal materials for solar-water evaporation and water-repellent coatings, using nanotechnology and nanomaterials, towards her doctoral degree under the guidance of Dr Aditya Kumar and Dr Apurba Sinhamahapatra.*

### 1. Introduction

Sunlight has an ultimate impact on life on Earth. Utilizing clean, renewable, and abundantly available solar energy is not a discovery to us but has been recognized to have diverse scope from the beginning. Advanced and appropriate solar energy utilization is the most affordable way to reduce the risk and



Apurba Sinhamahapatra

*Dr Apurba Sinhamahapatra is currently a Senior Scientist at the Water Resources Management (WRM) group, CSIR-Central institute of mining and fuel research (CSIR-CIMFR), Dhanbad, India. He received his BSC (Chemistry) degree in 2008 from the University of Burdwan and an MSc (Chemistry) degree in 2008 from IIT (ISM) Dhanbad. He pursued his doctoral study at CSIR-CSMCRI, Bhavnagar, and received a PhD (Chemical Science) in 2014 from AcSIR. Dr Sinhamahapatra has contributed over 40 research articles with an H index of 27. He and his group are actively working on nanoscale materials for wastewater treatment, solar evaporation, and artificial photosynthesis.*

cost involved in the existing practices to a greater extent. The research on solar energy and water evaporation has a long history.<sup>1,2</sup> From traditional solar basins to the modern concept of interfacial evaporation, it has received a surge of attention and interest among researchers, funding organizations, and policymakers.<sup>3–7</sup> Solar-driven interfacial water evaporation (SIWE) – a contemporary approach, is the most promising, with the highest evaporation rate recorded.<sup>8–12</sup> Water evaporation is a surface phenomenon resulting from liquid to vapor phase transition at the air–water interface benefiting from the surface energy localization. In SIWE, a solar absorber is placed at the air–water interface, making the process unique and appealing. Ideally, this thermally insulated solar absorber, called the SIWE device, efficiently absorbs solar energy and converts it to thermal energy. The thermal energy gets confined to the interface, heating the surface water rather than the bulk. Because of this lower conductive SIWE device, the heat lost pertaining to convection, radiation, and conduction from the device to the environment and the bulk is reduced. In return, the bulk water does not participate in solar water evaporation directly and maintains its temperature close to the ambient. In this way, this unique SIWE configuration focuses on the improvised localized heating at the liquid surface, engaging efficient solar utilization with enhanced light absorption capability of the absorber, thereby minimizing the heat loss from the absorber to the bulk water.<sup>13,14</sup> Fig. 1 demonstrates a schematic illustration of SIWE.

The superior functioning of SIWE lies over four key components – solar absorptivity of the absorber, adequate water transportation to the interface, appropriate heat management, and capability of scoring high water evaporation rate without undergoing fouling or salt accumulation-related problems over the absorber. This technology can quickly achieve a high photothermal conversion efficiency of more than 80%.<sup>15,16</sup> For instance, Zhou *et al.* presented a unique hydrogel-based

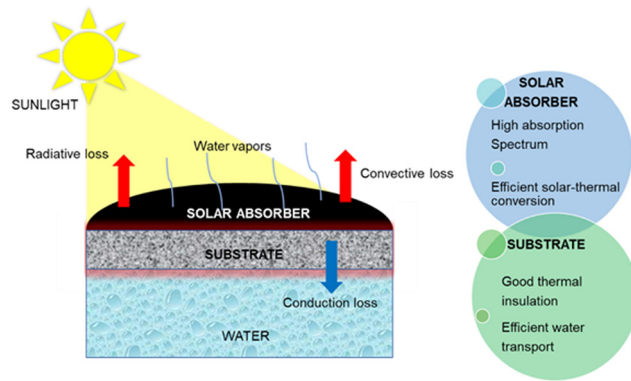


Fig. 1 Schematic illustration of solar-driven interfacial water evaporation.

antifouling solar evaporator for solar water desalination, facilitating improved water transport with minimized thermal losses.<sup>17</sup> Their design generates  $2.5 \text{ kg m}^{-2} \text{ h}^{-1}$  of water vapor with an efficiency of around 95% under one solar irradiation. Likewise, Wang and his team reported a water evaporation efficiency of 96.5% *via* a molybdenum carbide/carbon-based chitosan hydrogel (MoCC-CH).<sup>18</sup> Furthermore, Zhao *et al.* prepared micro-channelled hierarchically nanostructured gels (HNGs) *via* *in situ* polymerization of PVA and polypyrrole (PPy). The design remarkably reported a water evaporation efficiency of around 94%, with 18–23 liters of pure water collection per day.<sup>10</sup> Besides, a rapid expansion was seen in the solar water evaporation notion, furthering potential applications in various fields. These applications include wastewater evaporation, seawater desalination, electricity generation, chemical fuel production, solar steam sterilization, *etc.* They mostly come as complementary to clean water generation, utilizing the energy in other forms (thermal, electrical, chemical, *etc.*) for further sustainable usage. Liu *et al.* demonstrated a facile deflagration synthesis of hollow carbon nanospheres having excellent evaporation efficiency of 92.7% at one sun, with effective removal of impurities from various wastewater.<sup>19</sup> Likewise, there has been tremendous research done, including by Qu *et al.*,<sup>20</sup> Zhou *et al.*,<sup>21</sup> Wang *et al.*,<sup>22</sup> Shi *et al.*,<sup>23</sup> Jiang *et al.*,<sup>24</sup> Lee *et al.*,<sup>25</sup> *etc.*, which has been published in recent years under the utilization of solar energy with the ultimate goal of producing water and its implication in other diverse applications.

Several review articles have already been published and are under research, illustrating the basic design of the SIWE devices, their fabrication, effectual evaporation, and conversion techniques, especially the choice of appropriate materials and their working principles. But only a few discuss the other potential applications and their usage in real-life practices. This review starts with a brief introduction and discussion of the existing photothermal sheets and the different approaches in SIWE device fabrication. Herein, we sketch recent developments in their performance and other diverse applications regarding evaporation efficiency and solar-thermal conversion capability. They primarily include solar absorbers based on plasmonic nanoparticles (NPs), carbon-based



Aditya Kumar

*Dr Aditya Kumar is working as an associate professor in the Department of Chemical Engineering, Indian Institute of Technology (IIT-ISM) Dhanbad, India. He received his PhD from the University of Siegen, Germany, with a specialization in surface and interfacial engineering. Dr Kumar has published more than 65 peer-reviewed publications, several book chapters, and editorial-type scientific articles in various areas*

*of science and engineering. He is an associate editor of *Frontiers in Chemical Engineering* and *Frontiers in Nanotechnology*. He has edited and served as a scientific reviewer of numerous peer-reviewed journals and scientific organizations.*



materials, semiconductors, polymers, and hybrid/composite materials, and secondarily the supporting substrates, with strategized structural engineering. Besides these basic designs, this review outlines ways of solving the real-world issues, focussing on some key factors, including light localization, anti-scaling, long-term stability, cost performance, *etc.*, for designing a reliable solar water evaporator. We tried to delve into the inconsistency between the laboratory scale and the realistic conditions that allow the actual real-life practices. Altogether, this provides information on practical exposure underlying the significant problems with possible solutions concerning the aforementioned reports. Lastly, the prospect of the future solar evaporators and the possible development directions of solar water evaporation were proposed. We envision that this review highlights important points to improve the current solar evaporation systems and stimulate new ideas in this field.

## 2. Basic consideration in designing solar-driven interfacial water evaporation (SIWE) devices

Over the past decade, researchers have effortfully funded the development of SIWE devices largely concentrating on the air-water interface mechanism with high photothermal energy conversion efficiency. The photothermal materials as the solar absorbers, efficiently capable of absorption and conversion of solar energy to heat with the substrate, having properties including thermal insulation, and high porosity for the water transport facility, have become the key elements for these devices. In this section, we outline the recent progress and discuss the technical advancement of the solar water generation devices, studying various parameters including solar energy harvesting, heat utilization, water pathways, wettability, topography, and various others, thereby maximizing the evaporation rate and effectively reducing the overall heat losses.

### 2.1 Solar absorbers

Solar absorbers are photothermal materials with a wide range of solar spectrum absorption characteristics. Their ability to convert the captured solar energy to heat introduced them as the widely explored element in solar water evaporation. The photoexcitation of these materials is the primarily driven property in their functioning. They can be categorized into semiconductors, carbonaceous, polymeric, and plasmonic materials, and hybrid/composite materials working under a single or multiple mechanism (Fig. 2).<sup>26</sup> Furthermore, these mechanisms are: (i) plasmonic localized heating mechanism, modeled by plasmonic materials, (ii) electron-hole generation and relaxation mechanism, featured by semiconductors and lastly, (iii) thermal vibration of molecules-based mechanism, demonstrated by both the carbonaceous and polymeric materials (as shown in Fig. 3).

To begin with, plasmonic materials inherit a promising effect on solar-to-heat conversion efficiency, operating on

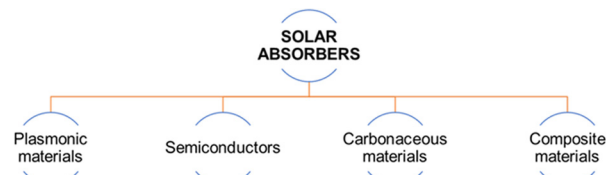


Fig. 2 Schematic diagram categorizing different solar absorbers used in SIWE devices.

surface phenomena with localized plasmonic heating mechanisms.<sup>27</sup> With investigation carried out over the years, the intrinsic narrow solar absorption spectrum established by these as-designed plasmonic NPs deters their application under broader wavelength light absorption, found as promising candidates for SIWE.<sup>28,29</sup> To date, various NPs have been reported to function well under plasmonic-based solar absorbers, such as Au,<sup>14,30</sup> Al,<sup>8</sup> and Ag.<sup>31,32</sup> Besides the narrow absorption spectrum and size distribution, researchers have encountered thermal stability as another concerning parameter in the plasmonic functioning of noble metals because of their loosely packed structures and high-temperature sensitivity<sup>30</sup> and hence this requires a promising solution that broadens the absorption band spectrum, increases the high temperature durability, and reduces the cost.

Carbon-based materials feature strong solar absorption capability and being black in appearance increases their solar-thermal conversion capability, making them the most suitable candidates for the SIWE system.<sup>33</sup> Among the various carbon-based materials reported, some with the properties of low cost, high absorption capability, and relatively stable and easy processing include graphene,<sup>34,35</sup> graphene oxide/reduced graphene oxide,<sup>36,37</sup> hollow carbon spheres,<sup>19</sup> carbon nanotubes (CNTs),<sup>38</sup> carbon dots,<sup>39</sup> carbon black,<sup>40</sup> *etc.* Although being the most promising photothermal materials with fabrication ease and better amalgamation with the substrate, their stability and the associated cost are common real-life challenges. However, recent advancements in the integrated evaporation design include polymeric sponge,<sup>41</sup> carbon sponge,<sup>42</sup> flame-treated wood,<sup>43</sup> and 3D fabrication printing techniques.<sup>44</sup>

The other photothermal material category is semiconductors with high tuneable energy levels and easy-to-access light-to-heat convertible thermalization. They are the materials that function as soon as the sunlight falls over them. Like carbon-based materials, their copious nature, low cost, and low toxicity make them widely explored solar absorbers. To be more elaborate, the mechanism includes the excitation of electron-hole pairs when photon energy higher than the band gap is incident on the surface and the relaxation of which before recombination on the two edges, namely the conduction and valence bands, results in promising irradiative energy conversion to heat.<sup>44</sup> A narrow band gap is generally preferred over a broader one for slower electron-hole pair recombination, facilitating higher solar-thermal conversion efficiency with appropriate solar energy utilization and enhanced light absorption



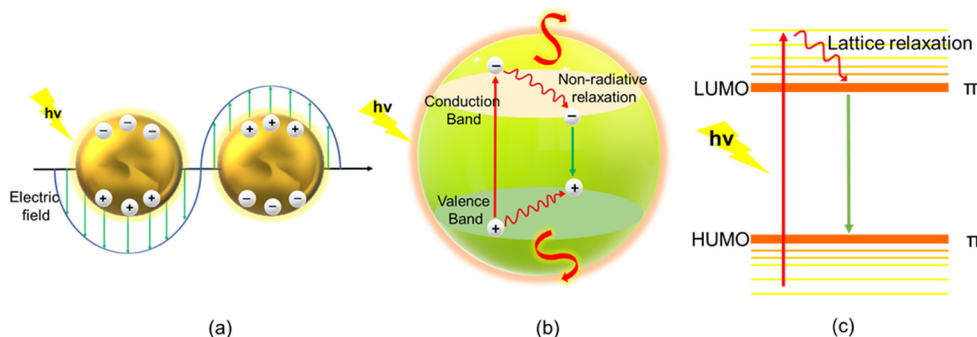


Fig. 3 Different possible photothermal mechanisms: (a) plasmonic heating, (b) electron–hole generation and relaxation, and (c) thermal vibration of molecules.

capability over a wider spectrum.<sup>45</sup> Under this category, we have materials such as black/reduced titanium dioxide,<sup>45,46</sup>  $\text{Ti}_2\text{C}_3$ ,<sup>47</sup>  $\text{MoS}_2$ ,<sup>48</sup>  $\text{Cu}_7\text{S}_4$  nanocrystals,<sup>49</sup> hierarchical copper phosphate,<sup>15</sup> etc., demonstrating effectual performance in the solar water evaporation systems. Other than these, the co-combination of metals to bimetallic forms, such as  $\text{ZnFe}_2\text{O}_4$  and  $\text{CoFe}_2\text{O}_4$ , and trimetallic forms, illustrated better system advancement.<sup>16,50,51</sup> Furthermore, some studies have demonstrated semiconducting absorbers with an improvised lowered band gap capable of harvesting enough heat with effective water evaporation under one solar irradiation.<sup>52,53</sup>

Polymers/conjugate polymers with delocalized  $\pi$ -electrons, split energy levels and under-control band gaps have high potential solar absorption characteristics.<sup>54,55</sup> Their adequate water transport facility<sup>56</sup> and easy modification *via* co-polymerization, or ionic or oxidative doping broadens the absorption spectrum leading to highly efficient light-to-thermal conversion.<sup>57,58</sup> Despite there being fewer options, the polymers that have been recently explored include polypyrrole (PPy),<sup>59,60</sup> polydopamine,<sup>61,62</sup> poly(1,3,5-hexahydro-1,3,5-triazines) (PHTs),<sup>63</sup> and hierarchically nanostructured gel (HNG)-based polyvinyl alcohol (PVA).<sup>10</sup> Another unique component is the polymer hydrogel that has recently emerged as a new platform for SIWE with higher absorption characteristics, effective heat utilization, lower energy demand, and anticipated structural engineering, promoting the future applications with higher enhanced results.<sup>64,65</sup>

Extensively, light absorption, photo-to-thermal conversion effectiveness, and the capacity to localize thermal energy at the water-air interface are three crucial factors to take into account when building photothermal materials. However, the individual functional solar absorbers fall short of providing full coverage. In order to create the optimal solar water interfacial device, composite materials—a combination of two or more different types of solar absorbers—become essential. In a similar context, Fang *et al.* prepared a self-floating flexible  $\text{W}_{18}\text{O}_{49}$ /carbon foam composite with an ability of water evaporation rate 6.6 times more than that of pure water.<sup>66</sup> Likewise, Tao *et al.* created a novel solar absorber using a composite material made of copper chalcogenide  $\text{CuS}$  nanoflowers that were encapsulated in a semipermeable nitrocellulose collodion

membrane (SCM). The device outperforms several existing materials and is inexpensive, simple to make, and environmentally benign.<sup>67</sup> Recently, Zhang *et al.* presented a highly effective solar-absorber composite material based on tetracyridylporphyrin, which produced thermoelectric power at a rate of about 60 mV and water evaporation at a rate of  $\sim 0.69 \text{ kg m}^{-2} \text{ h}^{-1}$  under  $1 \text{ kW m}^{-2}$  of solar radiation.<sup>68</sup> Similar to this, integrated cellulose-based composites,<sup>69</sup> novel photothermal materials based on the combination of  $\text{ZrO}_2$  nanoparticles (NPs) with Ni-doped carbon quantum dots (Ni@CQDs) and multi-walled carbon nanotubes (MWCNTs) coated on a melamine foam (MF) surface,<sup>70</sup> composite hydrogel (GO/SA PAM-PVA hydrogel),<sup>71</sup> and porous reduced graphene-agarose spherical composite<sup>72</sup>-based solar absorbers were reported with excellent evaporation efficiency and advanced functionalities. However, due to the complex nature and circuitous synthesis, the stability and scalability of these photothermal materials remain challenging in their successful functioning in future investigations.

Nevertheless, among all the photothermal materials, carbonaceous materials could be considered the most widely explored and practically preferred solar absorbers in the SIWE system. Their relatively low cost, copious nature, and diverse applications keep aside the other photothermal materials with their own sets of tailbacks toward practical applications, whether in terms of fabrication cost, limited scalability, stability, or toxicity. Furthermore, an ideal solar absorber seeks unique characteristics such as high solar absorbance, low thermal emissivity, and higher reflectivity towards the longer infrared wavelength with minor radiation loss.<sup>73</sup> Other than these, the choice of appropriate substrates, water management, evaporation structures, and solar water evaporation device design play a secondary role in efficient SIWE, which is discussed in further sections.

## 2.2 Substrates

Like the solar absorber, substrate materials have equal importance in efficient solar evaporation device design. The primary critical elements in the choice of the substrates include better water transport/evaporation facility and appropriate thermal insulation (as shown in Fig. 4). The efficient water transport or

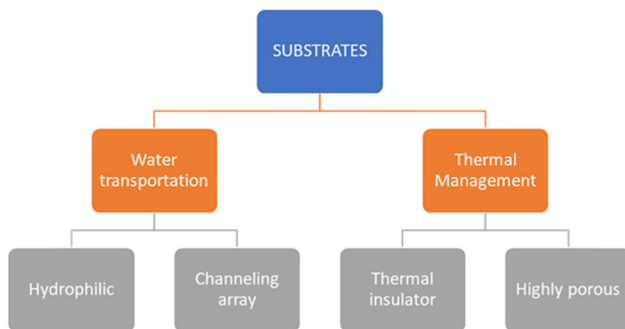


Fig. 4 Schematic diagram presenting substrates used in SIWE on the basis of the required decisive properties.

evaporation rate requires suitable wettability properties and continuous water pathways. In contrast, the second essential key element includes low thermal conductivity with a porous structure for improvised thermal insulation of the substrate. Herein, porosity is the common factor, favoring these essential vital elements and balancing the better functioning of the proposed device. For the same, researchers have investigated the individual functioning of the better water facility and the thermal insulation structure, which is discussed in more detail in the following sections.

To date, various substrates have been studied and developed. They possess excellent hydrophilicity (good wettability), low thermal conductivity, high porosity, and an effective channeling structure to facilitate better water transportation. They include cellulose foam,<sup>74,75</sup> polyurethane (PU) and polystyrene (PS) foams,<sup>76,77</sup> AAO,<sup>8</sup> GO aerogel,<sup>78</sup> air-laid paper,<sup>14</sup> CNT arrays,<sup>79,80</sup> natural wood,<sup>81,82</sup> cotton,<sup>83,84</sup> carbon fabric,<sup>85</sup> stainless steel,<sup>86</sup> etc. In general, an appropriate substrate with advanced water transport and thermal insulation will boost the SWE system to a greater extent.

### 2.3 Light absorption and heat utilization

Generally, the basic design principle a researcher looks at constitutes higher light absorption across the whole solar spectrum with excellent solar-thermal conversion efficiency. The other involves appropriately utilizing this thermal energy in the overall efficient system functioning. Henceforth, these two key objectives have become the primary steps in developing a high-performance solar water evaporator. The sunlight falling on the Earth's surface carries a wider wavelength from 300 nm to 2.5  $\mu\text{m}$ , including approx. 3% ultra-violet region (wavelength, 300–400 nm), approx. 45% visible region (wavelength, 400–700 nm) and the remaining 52% infra-red region (wavelength, 700 nm–2.5  $\mu\text{m}$ ). Additionally, an ideal performance could only be reached when the concerned absorber shows lower emissivity along with maximum solar absorption across the entire wavelength, especially the IR region, which comprises a higher percentage of the overall spectrum.<sup>73</sup>

Other than the material's absorption capability, morphing strategies can help in enhancing the absorptivity further.<sup>50</sup>

Recent review articles study these activities by introducing the micro/nanostructures in the absorber, enabling multi-internal reflection with longer optical path lengths for incident light resulting in enough absorption. Moreover, it also minimizes the transmittance and emission level of the concerned absorber.<sup>87–90</sup> Another vital observation includes a strong correlation between efficiency and semiconductors and their band structures. The element doped over the absorber decreases the band gap energy with lower recombination of the electron-hole pair, broadening the absorption wavelength and eventually helping in better light absorption tendency.<sup>53</sup>

Furthermore, the energy the absorber receives is converted to heat, which gets steadily transferred to the bulk, thereby instigating the phase transition from liquid to vapor. This utilization of heat in the SIWE system can be divided into three major parts, comprising (i) energy powering water evaporation, (ii) radiative energy lost from solar-thermal converting materials, and (iii) convection and conduction heat lost to the environment *via* non-radiative energy dissipation.<sup>91</sup> The former plays a vital role in presenting the overall efficiency of the SIWE system, while the latter is subjected to be minimized, enhancing the former. This conversion efficiency possibly is determined by the ratio of the stored thermal energy in the generated vapor to the amount of solar energy incident on the device, which is calculated as,

$$\eta_{s-v} = \frac{\dot{m}h_{LV}}{C_{opt}q_i} \quad (1)$$

Or,

$$\eta_{s-v} = \frac{Q_t}{C_{opt}q_i} \times \frac{\dot{m}h_{LV}}{Q_t} \quad (2)$$

$$\eta_{s-v} = \eta_{s-t} \times \eta_{t-v} \quad (3)$$

where  $\dot{m}$  refers to the evaporation rate of water,  $h_{LV}$  refers to the enthalpy of vaporization,  $q_i$  is the nominal solar irradiation value (*i.e.*, 1  $\text{kW m}^{-2}$ ), and  $C_{opt}$  represents the optical concentration. Furthermore, the solar-vapor conversion efficiency  $\eta_{s-v}$  is summarised as the product of solar-thermal efficiency  $\eta_{s-t}$  and thermal-to-vapor efficiency  $\eta_{t-v}$ . The equation above is the most common characterization of SIWE efficiency calculation.<sup>8,92</sup> It is easy to understand from the energy balance viewpoint. Here, when the input heat is the same and the heat loss is the same, the neat energy added to the system (water) is balanced by the same amount of evaporation enthalpy taken away by the generated water vapor.<sup>93</sup>

Under a similar principle, for a steady-state operation, different researchers define the system differently.<sup>45,94,95</sup> Hence, there is no such standard formula. Moreover, in a transient state, the critical variables upon which the conversion is based keep diverting depending on the changing climatic conditions and even the materials respond differently. Consequently, it becomes tricky and sometimes confusing to evaluate and compare reported conversion efficiencies.<sup>96,97</sup>



## 2.4 Water management and its design

Continuous and effectual water movement from the bulk of the liquid to the heating surface is another essential requirement for the efficient functioning of the SIWE system. Despite the earlier studies, whether it is the choice of the absorber, substrate, or its proper solar utilization, better water transport facilities with their controlled activity can be categorized into – 1D, 2D, and 3D water pathways.<sup>91</sup> As depicted in Fig. 5(I), the 1D water pathway can be idealized with high thermal utilization efficiency, overcoming the conventional bulk heating and avoiding significant heat losses to the system. Likewise, nature-inspired designs based on mushroom,<sup>98</sup> jellyfish,<sup>99</sup> or rose<sup>100</sup>

demonstrate unique reports as well. Despite proving their efficient SIWE functioning, the low speed of the water approaching the heating surface, and the limited water evaporation rate, they direct towards higher dimensions, *i.e.*, 2D systems, and further 3D system design. In the 2D system, the presence of an insulator blocks the water transport, thereby minimizing the conduction heat loss and allowing the side capillary wicking mechanism for water evaporation. This type exhibits a more substantial capillary wicking effect, faster water transport, and directing effective solar water evaporation mechanism.<sup>100</sup> Furthermore, the unconventional 3D pathway with an interconnected pore structure is recommended for

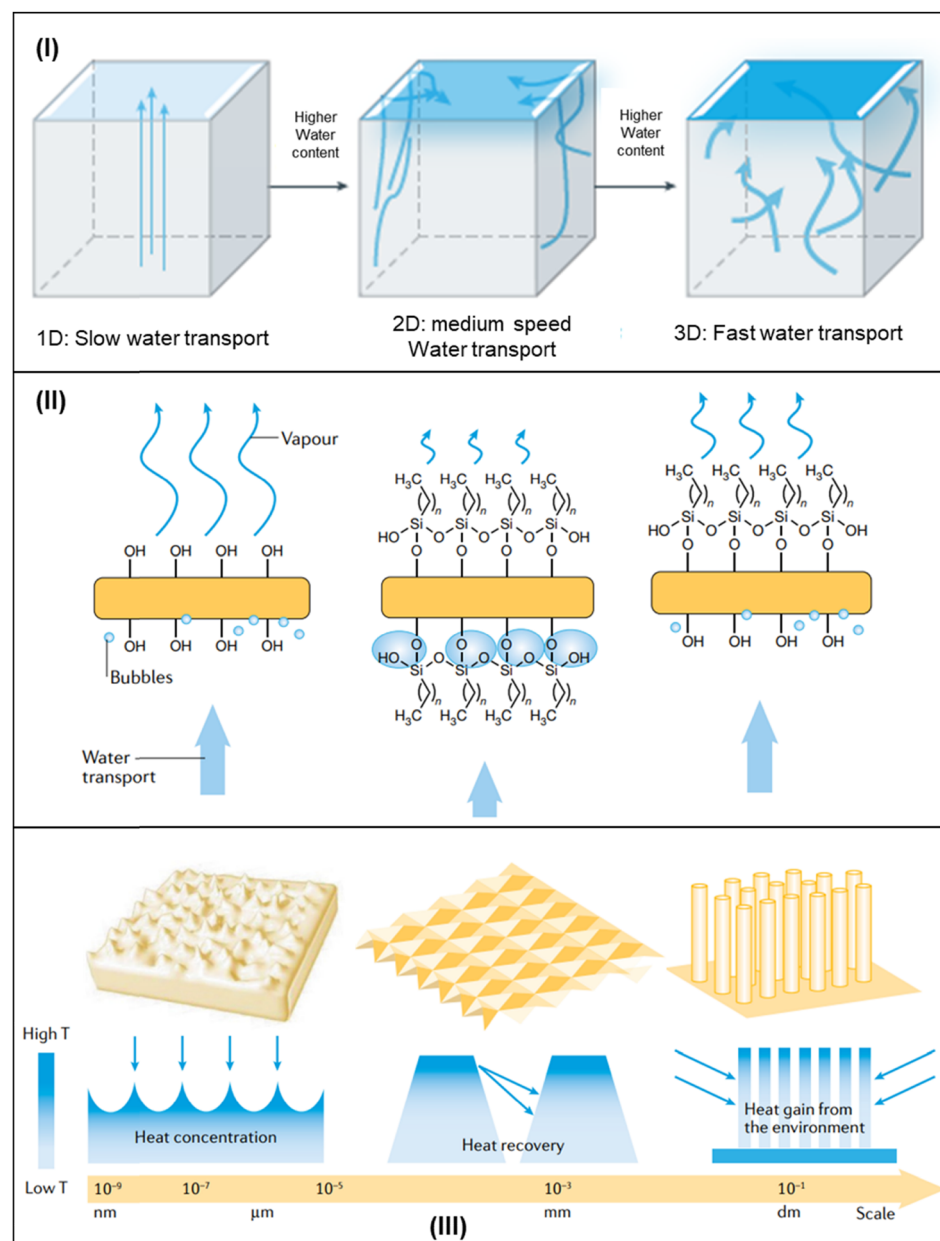


Fig. 5 (I) Water pathways – 1D, 2D, and 3D, (II) schematic of wettability ability on SIWE devices – (a) hydrophilic, (b) hydrophobic, and (c) their combined form, and (III) schematic diagram illustrating the tailoring of the topology influence on the SIWE device fabrication. Reproduced with permission.<sup>91</sup> Copyright 2020, Springer Nature.



more rapid water transport than the earlier dimensions. For the 3D water pathway – although it is the more advanced form with a prominent water facility, the pores present directly in contact with the water deteriorate the localized heating effect, thus fading the essential principle of the SIWE system.<sup>101</sup> And hence, the pores present in the as-proposed SIWE sample are designed to meet the essential requirement of both water transport and thermal insulation. For instance, the pores should be closed to minimize heat losses, whereas open pores are necessary for sufficient and continuous water transport. So, whatever the dimensions, the combined optimized result of water transport and thermal insulation incites the efficient functioning of the SIWE system.<sup>75,81</sup>

## 2.5 Structural and interfacial engineering

An adequately designed SIWE device with localized and interfacial heating properties becomes the key to achieving a higher performance rate with enhanced efficiency. Besides the appropriate pore sizes, floatability, and more substantial capillary wicking effect (as discussed in earlier sections), wettability plays a dynamic role in the SWE system, especially when dealing with the interfacial characteristics of the device with the water in the bulk. However, recent studies summarise the free-standing interfacial evaporation system to be categorized separately based on wettability properties – hydrophilic, hydrophobic, and a combination of both at the top and the bottom surfaces (Fig. 5(II)).<sup>91</sup> Being too much of one kind could lead to mechanical failure. For example, considering the continuous water transport and capillary wicking effect, hydrophilicity proves to be the best, theoretically. But the extreme hydrophilicity leads to excessive water pumping, resulting in heat loss with issues questioning its flexibility and fouling.<sup>100</sup>

On the other hand, the hydrophobic surface tries to efficiently establish its functioning in the SIWE system with excellent floatability, self-cleaning, self-healing properties and highly durable and stable characteristics; for example, the fluoroalkyl silane PPy-coated mesh, TiO<sub>2</sub> coated stainless steel mesh, carbon-coated gauze, etc.<sup>60,86,102</sup> Still, this design's limitations are inadequate evaporation rate, deficient water transport due to the un-wetting properties of the hydrophobic device, and further limited heat supply through conduction. With these observations, the generation of the Janus absorbers came into account, having both wettability properties with focussed objectives. These absorbers have a hydrophobic top surface along with a hydrophilic bottom. A recent study by Zhu *et al.* prepared a durable, highly efficient, and stable Janus membrane containing CB and PMMA over the hydrophilic end of PAN.<sup>103</sup> Another recent research study projected a bio-inspired soot-deposited Janus fabric as a promising and portable SIWE device, exhibiting a sustainable water evaporation rate of 1.375 kW m<sup>-2</sup> h<sup>-1</sup> with an efficiency of 86.3% under one solar radiation.<sup>104</sup> Henceforth, the construction of these bilayer Janus films can be represented as an effective strategy, achieving stability and a high evaporation rate for advanced water evaporation applications.

Further attention is drawn to the structural design of the SIWE devices that are designed or tailored to the absorber's topography, which can substantially impact the conversion efficiency, resulting in higher outcomes. Such a study of topography over the as-proposed solar absorber design significantly not only deals with the reduction of water content over the absorber side, but also provides a larger surface area to the absorber, increasing its absorption capability. Giving more area to the absorber reduces the bulk temperature compared to that of the environment. This forecasts the shifting of the evaporation surface from the nanoscale to the macroscale, thereby enabling the heat recycling provision of the system (Fig. 5(III)). Recent research compared the effect of the morphed surface with that of the flat one on the PVA hydrogel, where the former shows an evaporation rate of 45% more than the latter.<sup>105</sup>

Similarly, the highly configured periodic pattern structures at a small scale reduce the reflectance at a higher level with more extensive evaporation provision, resulting in astonishing conversion efficiency. Another important term recovered recently is origami, whose mountain-like structure shows impressive results while dealing with heat loss recovery. Their unconventional 3D patterns, exceptional sunlight trapping capability, and more illustrative evaporating surfaces prove them to be the ideal engineering with full solar irradiation utilization.<sup>106,107</sup> Additionally, the presence of active water molecules or, in other words, the hydration of solutes in the liquid or variation in water state powers up the evaporation process with a subtle decrease in energy demand, looking for materials with the desired properties, faster and enhanced solar water evaporation efficiency.<sup>65</sup>

## 3. Distinguishing SIWE materials for different applications

Based on the aforementioned analytics, we focus our discussion on several SIWE device applications, such as water purification, electricity generation, steam sterilization, oil-spill clean-up, solar fuel production, and many more, using the diverse evaporating materials in use (as shown in Fig. 6).

### 3.1 Water evaporation and desalination

Almost one-fifth of the world's population is living under water scarcity and another 1.6 billion people live under economic circumstances, mainly due to the technical or financial boundaries of getting fresh water. This demands an onset of technology, fulfilling the combined advantages, including freshwater generation, easy accessibility, and a cost-efficient energy input globally dealing with the water crises worldwide. Solar energy being copious in nature and in combination with water could eventually move forward in response to the water scarcity issues with lower environmental impact. The same can be observed whether it is salt harvesting, desalination, or steam generation. This solar-enabled water treatment method is considered a more attractive and sustainable approach for producing clean water, converting non-drinkable water sources, such as





**Fig. 6** Schematic diagram illustrating various potential applications of the SIWE device. Plasmonic materials. Reproduced by permission.<sup>8,30</sup> Copyright 2016, Springer Nature. Copyright 2016, American Chemical Society|| Carbonaceous materials. Reproduced by permission.<sup>4,108</sup> Copyright 2014, Nature. Copyright 2017, Royal Society of Chemistry|| Semiconductor. Reproduced by permission.<sup>48,109</sup> Copyright 2019, Royal Society of Chemistry. Copyright 2020, American Chemical Society|| Polymers. Reproduced by permission.<sup>10,60</sup> Copyright 2018, Nature. Copyright 2015, Wiley-VCH|| Desalination. Reproduced by permission.<sup>110</sup> Copyright 2021, Royal Society of Chemistry|| Solar fuel production. Reproduced by permission.<sup>111</sup> Copyright 2009, American Chemical Society|| De-icing. Reproduced by permission.<sup>112</sup> Copyright 2018, American Association for the Advancement of Science|| Steam generation. Reproduced by permission.<sup>113</sup> Copyright 2017, Royal Society of Chemistry|| Oil-spill cleanup. Reproduced by permission.<sup>114</sup> Copyright 2020, Royal Society of Chemistry|| Electricity generation. Reproduced by permission.<sup>115</sup> Copyright 2018, Elsevier.

seawater, river/lake water, or contaminated water, to usable/drinkable water, to a greater extent.<sup>9</sup> Here in this section, we discuss various research studies on different materials based on solar-driven interfacial water evaporation (SIWE) devices, reported to date with their accomplishments and challenges.

**3.1.1 Plasmonic-based SIWE devices.** In the field of solar-water evaporation, researchers have preferred plasmonic materials because of their extensive overlapping response over the visible and IR spectra. It is reported that these material-based evaporators can enhance light absorptivity and work on the mechanism of localized heating, thereby increasing the system's overall efficiency. For example, Zhu *et al.* proposed a portable, scalable floating absorber with an overall solar absorption efficiency of 96%, water evaporation efficiency of around 90%, and effective desalination. The absorber was prepared by self-assembling Al nanoparticles into a commercially available 3D porous membrane, as shown in Fig. 7.<sup>8</sup> They demonstrated their design as an effective, efficient, portable, and personalized solution to solar water desalination. Furthermore, with a stable and long-term desalination proposal, Zhang *et al.* developed a flexible and mildew-resistant aerogel coated with Au NPs, with a high absorption efficiency and evaporation rate of about  $1.394 \text{ kg m}^{-2} \text{ h}^{-1}$  under one sun. The system was reported to have run a continuous cycle of 120 h, exhibiting repetitive self-cleaning behavior and excellent stability.<sup>116</sup>

Although exclusively explored, the high cost of these materials makes them unattractive for a large-scale system. Hence, Traver and his team studied a scalable and sustainable method. They compared plasmonic metal nitrides over the AAO interface for water desalination to reach new and inexpensive plasmonic NPs for SIWE, out of which the HfN-AAO interface with 95% solar-thermal conversion efficiency successfully achieved a water evaporation rate of about 87% under one solar radiation with effective removal of major metal ions, with ocean water as the source.<sup>117</sup> Li and his team fabricated a bilayered polymer foam-based SIWE device, with remarkable efficiency greater than 90%. Furthermore, the system presented other additional properties such as stability, scalability, anti-fouling, and reusability.<sup>118</sup> Hence, it can be noted that water evaporation or desalination using plasmonic nanostructures, *via* harnessing the solar input and converting it to the requisite heat, is gaining interest as a scalable and sustainable method to address global freshwater scarcity to a greater extent.

**3.1.2 Polymer-based SIWE devices.** In the practical applications of water evaporation from saline water, the hydrophobicity of the absorber is maintained using different surface modifiers. Because of this, the highly oxidative chemicals in air and water react on being exposed to sunlight, often resulting in worsening of the hydrophobic characteristics, leading to hydrophilic wettability of the materials in a few uses. Therefore, there comes the requirement of a self-healing hydrophobic photothermal material that can autonomously recover its hydrophobicity characteristics. In response to the above, Wang and his co-workers fabricated a self-healing hydrophobic photothermal sheet using polypyrrole over stainless-steel mesh with a conversion efficiency of 58%, self-healing capability, broader absorption spectrum, and excellent photothermal properties, which in turn permits an automated and uninterrupted interfacial solar heating.<sup>119</sup> The noticeable results with polymeric sheets as absorbers have also been observed in desalination applications. For instance, Li *et al.* created a SIWE device using PPy coating over CMCA (P-CMCA) having hierarchical channeling, showing excellent conversion efficiency of 96.8% under one sun irradiation. In addition, the device showed extraordinary efficiency of 94.7% (20 wt% NaCl) salt-resistant performance with accumulation hindrance for 30 days. The presented design has outstanding long-term stability and is a promising competitor.<sup>120</sup> In a similar manner, PPy-coated VMP monolith shows an abundant macroporous structure, cost-effectiveness, super-hydrophilicity, and low thermal conductivity and ideal mechanical properties, making it a promising platform for solar steam generation – energy efficient with salt rejecting qualities, as shown in Fig. 8.<sup>121</sup>

Other than these, there are various other reports justifying the excellent working of PPy over any type of porous substrate, such as over cotton fabric,<sup>122</sup> wood,<sup>123</sup> in aerogel form,<sup>64</sup> etc. Moreover, a modified PU sponge, an artificially designed mushroom-based PVA sponge with charcoal coating, demonstrated noticeable results, opening doors to the next generation thermal desalination membranes utilizing an abundantly available water resource and, free of cost solar energy.<sup>124</sup>

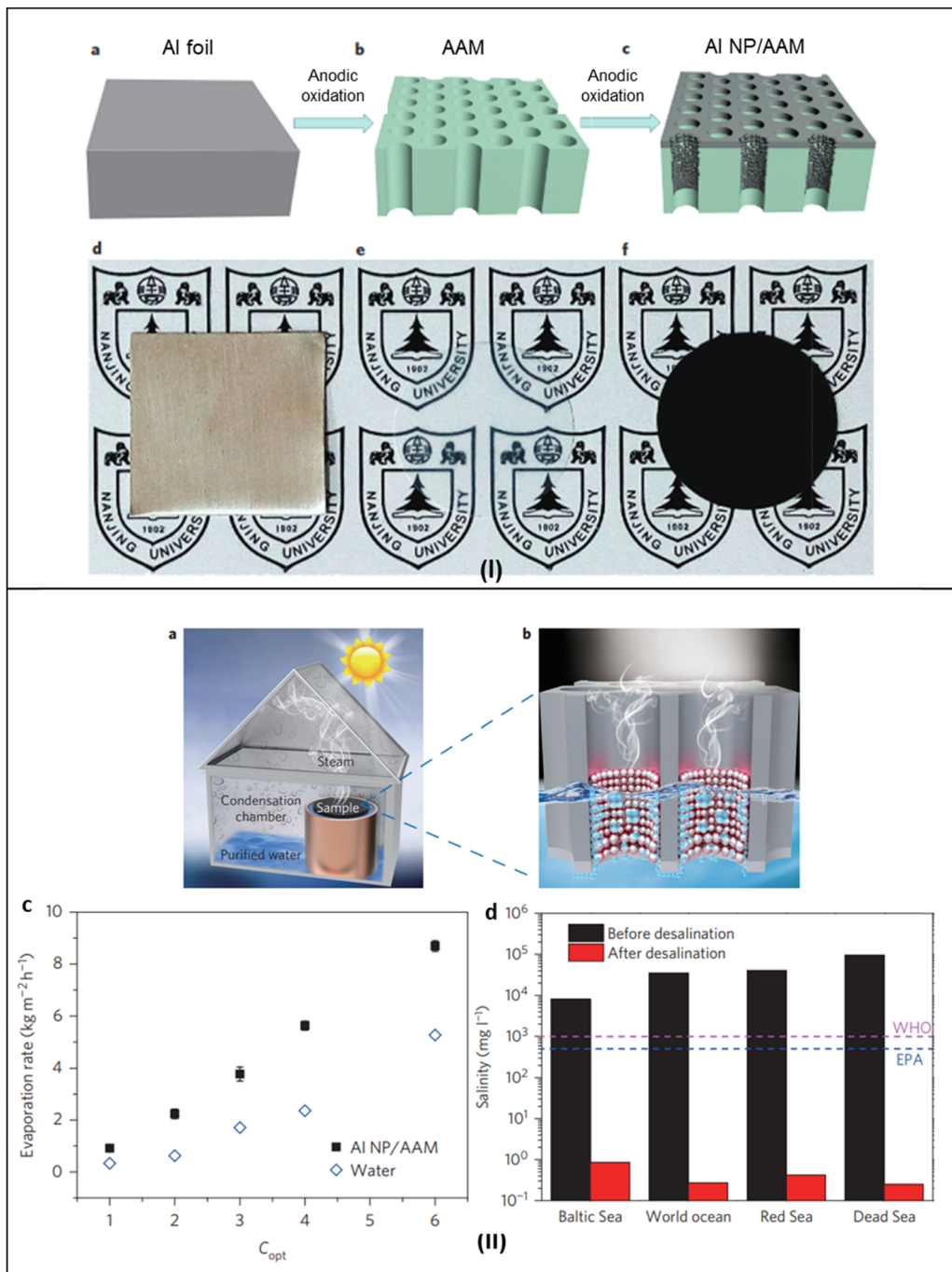


**Fig. 7** Plasmonic-based water purification SIWE devices; (I) fabrication process of the Al NP-based plasmonic structure and (II) (a) and b) set-up and schematic of plasmon-enhanced solar desalination, (c and d) performances based on mass change and evaporation rate achieved, respectively. Reproduced with permission.<sup>8</sup> Copyright 2016, Springer Nature.

**3.1.3 Semiconductor-based SIWE devices.** In the industrial applications of SIWE devices, engineers seek a broader absorption spectrum capability of materials with high absorption, less transmission, and reflectance characteristics. On the other hand, this can be shrouded with semiconductors. Their stability, economy, and intrinsic properties make them one of a kind. Black/reduced titanium, a hydrogenated metal oxide, emerges as the most identified solar absorber with higher

solar-thermal conversion efficiency and better solar-driven interfacial evaporation performance for different applications.<sup>125</sup> Among other methods employed, introducing oxygen vacancies and generation of black  $TiO_2$  are effective strategies for narrowing the band gap and thus enhancing the light absorption capability.<sup>22</sup> For instance, the experimental investigation made by Ye and his co-workers tested the performance of the as-synthesized  $TiO_x$  NPs spin-coated onto the



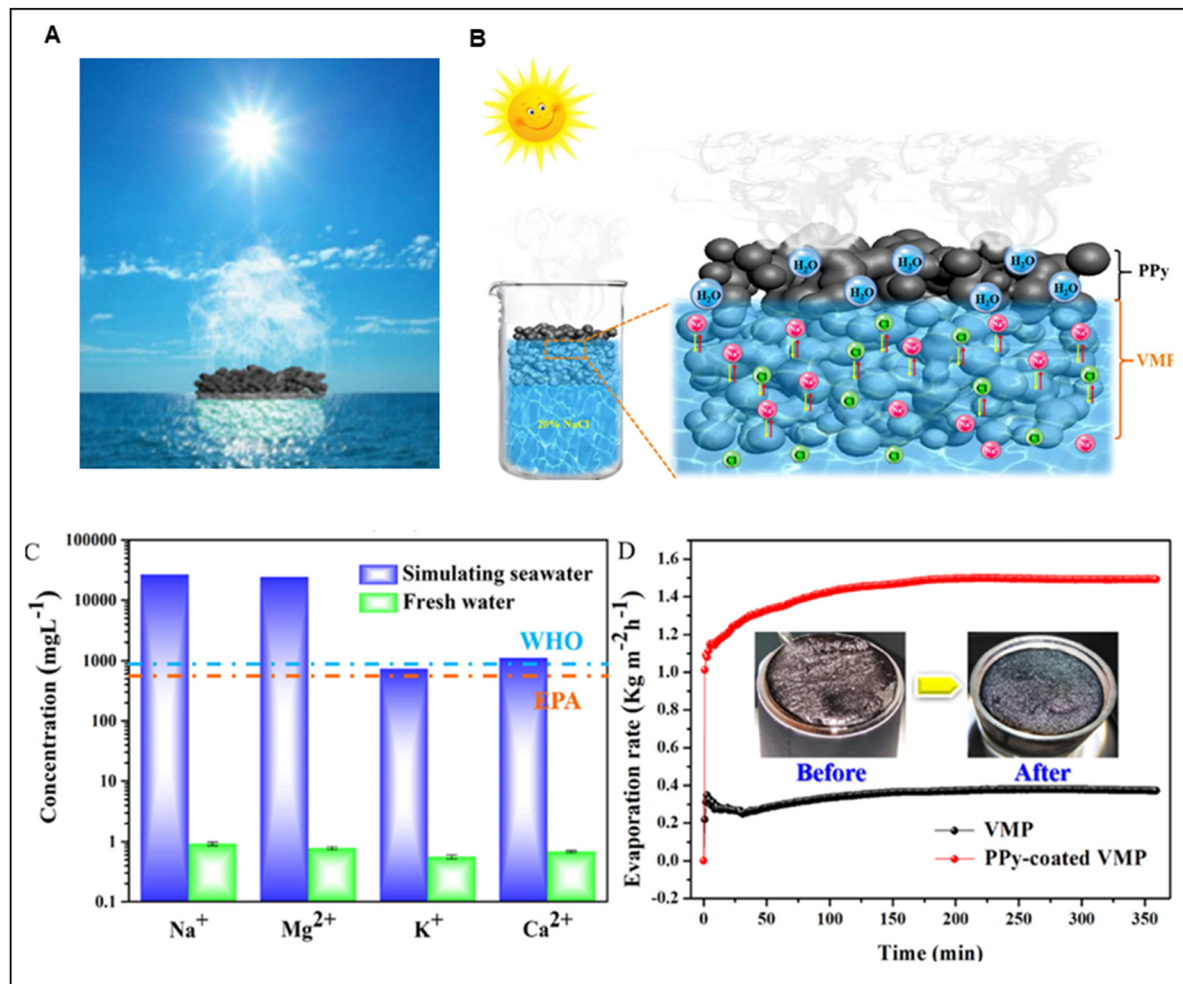
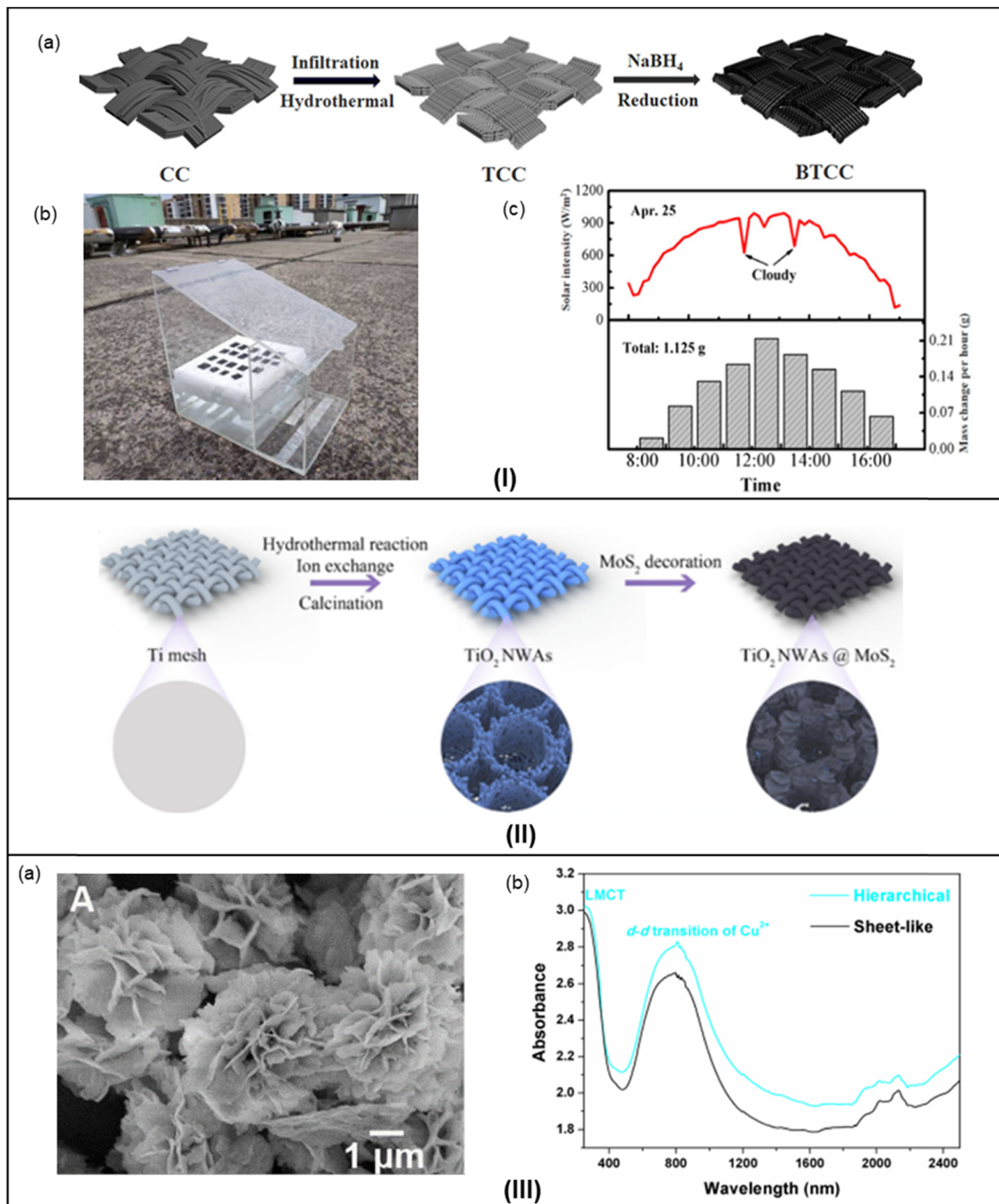


Fig. 8 Polymer-based water purification SIWE device. A PPy-coated VMP solar steam generator: (A and B) schematic diagram and structure of the device, (C) concentrations of cations in simulated seawater and distillate; the colored dashed lines denote the WHO and EPA standards for drinkable water, and (D) time-dependent steam evaporation rate in 20 wt% NaCl solution with one sun irradiation. Reproduced with permission.<sup>121</sup> Copyright 2020, American Chemical Society.

surface of an SS mesh followed by surface superhydrophobization and working as a steam evaporator, with an evaporation capacity of about 50% under one sun intensity.<sup>45</sup> Also, when the researchers studied titanium gauze with reduced  $\text{TiO}_2$  nanotubes on the surface for air–water interface solar heating, the results were optimistic, opening routes for more advanced applications such as salt production and desalination.<sup>126</sup> Recent research on semiconductors demonstrated SIWE devices with more than 98% absorption and more than 90% conversion efficiency with an engineered-photothermal nanocomposite sheet called E-PNS (black  $\text{TiO}_2$ /polymer matrix). The system was reported to achieve clean water production at a rate of  $\sim 2.2 \text{ L m}^{-2} \text{ day}^{-1}$ , *i.e.*, 2.2 times higher than that with the blank water itself. This study aimed to offer an upcoming technological solution for producing clean water in water-scarce regions.<sup>127</sup>

Moreover, black titanium dioxide's unique nanocage structure has been synthesized for solar desalination.<sup>115</sup> Zhu and his team investigated the increased absorption capability, self-

floating, thermal stability, well-crystallized interconnected nanograins for better permeation, and other ideal characteristics within its nanocage structure and the report suggested solar–thermal conversion efficiency of more than 70.9% under simulated solar light with an intensity of  $1 \text{ kW m}^{-2}$ , inspiring new black materials with a rationally designed structure for superior solar desalination performance. Problems still prevail with many investigations and challenges, such as single decontamination function, relatively low efficiency, and inability for practical applications. Furthermore, a bioinspired moth-eye-like nanostructure was engraved over a carbon cloth using black titania (BT), demonstrating an impressive solar steam efficiency of about 94% under one sun illumination. Besides, the system subsequently underwent desalination, steam generation, and photocatalytic degradation. There single BTCC nanocomposites and large area BTCC nanocomposites still produced 1.125 g and 21.72 g of clean water, respectively, in the ever-changing environment, indicating the survival of BTCC nanocomposites still with higher performance in real-life



**Fig. 9** Semiconductor-based water purification SIWE devices. (I) BTCC nanocomposites, (a) schematic illustration of the preparation, (b) schematic illustration of the outdoor test using BTCC nanocomposites, and (c) the mass change of evaporated water per hour and the corresponding actual solar intensity. Reproduced with permission.<sup>46</sup> Copyright 2018, American Chemical Society. (II) Hierarchical 1D/2D TiO<sub>2</sub>@MoS<sub>2</sub>, schematic illustration of the preparation process. Reproduced with permission.<sup>128</sup> Copyright 2021, Elsevier and (III) HCuPO–PDMS composite sheets, (a) SEM images of HCuPO and (b) UV-vis-NIR diffuse reflection spectra of copper phosphate powder with different morphologies. Reproduced with permission.<sup>15</sup> Copyright 2017, American Chemical Society.

conditions (Fig. 9(I)).<sup>46</sup> With further advancement, Yuan *et al.* created a multifunctional solar absorber for sun-driven interfacial water evaporation and organic pollutant removal by fabricating 2D MoS<sub>2</sub> nanosheets ornamented on 1D TiO<sub>2</sub> nanowire arrays *in situ* formed on a Ti mesh (Fig. 9(II)) *via* microstructure engineering. Along with the superior

photodegradation performance, the as-proposed SIWE device was recorded to possess about 96.5% light absorption efficiency and an optimal evaporation rate of 1.42 kg m<sup>-2</sup> h<sup>-1</sup> under one sun irradiation.<sup>128</sup> Recently, a nature-inspired bifunctional micro-reactor recorded a high-water evaporation rate of 37.0 kg m<sup>-2</sup> h<sup>-1</sup> along with a high energy conversion efficiency



(91.2%) under simulated sunlight having the intensity of about  $25.5 \text{ kW m}^{-2}$ . Moreover, the  $V_{\text{oc}}$  removal rate (80.9% in 40 min) was recorded efficiently.<sup>129</sup>

Out of the other promising materials, copper and some of its compounds cross all the limitations, such as being cost-effective, having a sharp temperature gradient, and long-term photostability. Copper has emerged with excellent results due to its strong Vis-NIR absorption, mainly due to the d-d transition of  $\text{Cu}^{2+}$ . To exemplify the hierarchical micro-structured copper phosphate (HCuPO), Hua *et al.* and his team designed a solar absorber over porous PDMS sheets to accelerate water evaporation further. The evaporation rate of saline water (3.5 wt%) was measured to be in the range of  $1.13\text{--}1.85 \text{ kg m}^{-2} \text{ h}^{-1}$ , which was 2.2–3.6 times with a solar-thermal conversion efficiency of 63.6% that for the ordinary saline water without HCuPO, all under one sun intensity (Fig. 9(III)).<sup>15</sup> Another recent investigation proposed a Cu-based multifunctional photo-thermal material with abundant CuO nanowires. In this, the as-prepared multifunctional CuO nanowire mesh reported having high solar absorption of about 93%, excellent capillary action, and conversion efficiency of 84.4% under one sun illumination. This system allowed the incorporation of solar evaporation with pollutant degradation and antibacterial activity, holding great application potential in pure water production.<sup>130</sup>

Furthermore, with an idea to develop a scalable, affordable system with practically stable evaporation and salt-resistant performance, Zhang *et al.* demonstrated a highly scalable customizable practical application of copper-based SIWE device, with an efficiency of 98.5% and stability above 40 cycles. This bilateral evaporation system comprises CuS-bacterial cellulose (BC) hybrid gel membranes wrapped around PE foam.<sup>131</sup> The researchers showed that this flexibility and portability showed the system's uninterrupted salt-resistant properties for more than 12 h with a stable evaporation rate.

**3.1.4 Carbon-based SIWE devices.** The efficiency of the SIWE system depends strongly on the absorber's absorption capacity and as discussed earlier, carbon is the most favorable and is primarily being explored. Its ultra-high solar absorbance capability, stability, cost-effectiveness, and easy availability with high solar-thermal conversion efficiency make it technically vital in SIWE. Over the years, researchers have demonstrated vast diversity in their structure, from 1D to 3D design or single layer to multi-layered. For instance, there are various reports of single-layered carbon-based SIWE devices, among which a few include floatable hollow carbon nanospheres,<sup>19</sup> porous graphene,<sup>44</sup> carbon dots,<sup>132</sup> graphene oxide-based aerogels,<sup>133</sup> carbon-loading support systems of reduced graphene oxide within the porous air-laid paper,<sup>134</sup> carbon black-based super-hydrophobic gauze,<sup>102</sup> microporous cokes in zeolite catalysts,<sup>135</sup> and porous polymers coated with exfoliated graphite.<sup>136</sup> All show excellent performances in respect of each other. Recently, Wang and his team fabricated a biomimetic ultra-black sponge (BUBS) with vertically aligned carbon nanosheets on a loofah sponge. With properties such as anti-reflection and wettability, the BUBS proved to be an efficient fabrication with the highest evaporation rate of  $1.93 \text{ km m}^{-2} \text{ h}^{-1}$

and about 98.5% evaporation efficiency under one sun. The system showed excellent performance in freshwater generation and desalination.<sup>137</sup>

Similarly, dual and multi-structured devices play a dynamic role in SIWE performance enlargement. A recently published report by Chen and his co-workers used exfoliated graphite over a carbon foam as a heat barrier, facilitating thermal insulation and the required capillary movement to the device. It was recorded to achieve a solar-thermal conversion efficiency of 85% with irradiation of around  $10 \text{ kW m}^{-2}$ , 2.4 times more than the conventional bulk heating.<sup>4</sup> Likewise, a flexible and scalable heat-localized solar desalination film with anti-clogging properties based on graphite was prepared by Ghasemi and his team (Fig. 10(I)). In a long-term performance, the system demonstrated five orders of desalination of extremely salty brine ( $1.52 \times 10^5 \text{ mg L}^{-1}$ ) with no decrease in its efficacy.<sup>108</sup> Furthermore, in a one-step process, Qi *et al.* proposed a carboxylated multi-walled carbon nanotube (MWCNTs-COOH) loading on the cotton fabric (CF) – the evaporation layer acted as the body and cotton yarns (CYs) as the tentacles used for water transportation, assembled altogether as a complete solar evaporator inspired from the jellyfish shaped body. This bio-inspired evaporator exhibited an evaporation rate of  $1.18 \text{ kg m}^{-2} \text{ h}^{-1}$  and a high energy conversion efficiency of 86.01% under 1.0 sun illumination (as demonstrated in Fig. 10(II)).<sup>138</sup> Similar investigations were reported, such as graphene/carbon cloth,<sup>139</sup> GO/cellulosic filter paper,<sup>76</sup> carbon black/cotton gauze,<sup>102</sup> etc.

Besides pure water production, various bilateral systems presented a practical desalination approach to SIWE. For example, Ren *et al.* used a hierarchically structured graphene foam as a SIWE device, whose porous and superior omnidirectional light harvesting performance showed a solar-thermal conversion efficiency of up to 93.4% and solar-vapor conversion efficiency of more than 90% for seawater desalination under high endurance.<sup>12</sup>

Moreover, with a more advanced structure, Xia *et al.* developed a novel self-rotating CNT-based, energy-efficient solar evaporator, demonstrating an ultrahigh salt tolerance ( $300 \text{ g L}^{-1}$ ) *via* periodic self-regeneration in hypersaline brine (as shown in Fig. 11(III)). The design illustrated a continuous operation cycle, “evaporation–crystallization–self-generation,” opening a way for reliable, practical applications. Additionally, when operated under different operational conditions, the system showed favorable outcomes, solving the universal salt fouling problem.<sup>141</sup> Utilization of CNT membranes as a light-absorbing layer was a frequent choice of many researchers due to their remarkable light-absorbing capability and profound structure. Accordingly, Xiong *et al.* created a single-layer photothermal membrane based on carbon nanotubes and employed it for SIWE with increased desalination efficiency (as shown in Fig. 10(III)).<sup>140</sup> Another article demonstrated a water lily-inspired hierarchically structured SIWE device enabling efficient evaporation ( $\sim 80\%$  solar-to-vapor efficiency) out of high-salinity brine (10 wt%) and wastewater containing heavy metal ions (30 wt%). More notably, neither a decrease in



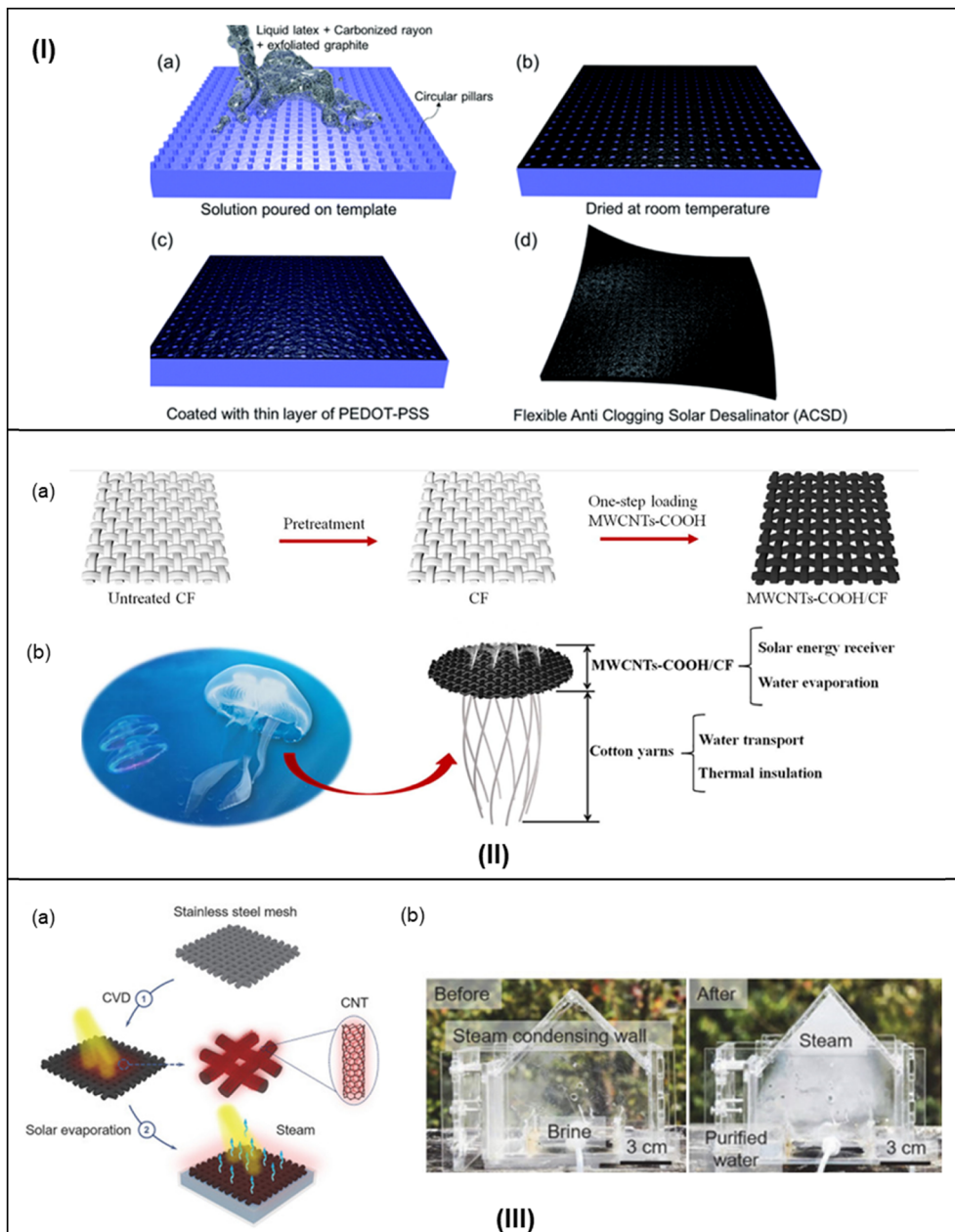


**Fig. 10** Carbon-based SIWE devices. (I) Solar desalination *via* flexible graphite film (a–c) schematic representation of the fabrication of the ACSD (anti-clogging solar desalinator). Reproduced with permission.<sup>108</sup> Copyright 2017, Royal Society of Chemistry. (II) MWCNTs-COOH/CF solar evaporator. (a) Preparation, and (b) representation of the inspiration for the designed system. Reproduced with permission.<sup>138</sup> Copyright 2020, Elsevier. (III) Single-layer CNT-based photothermal film. (a) Schematic diagram of the preparation process and evaporation *via* the prepared film and (b) the practical applications before and after the operation. Reproduced with permission.<sup>140</sup> Copyright 2020, Acta Physico-Chimica Sinica.

evaporation rate nor fouling on the absorbers was observed during the entire evaporation process until water and solute were separated. With the capabilities of stable and high-rate evaporation out of high-salinity brine and the effective separation of solute from water, this technology has high expectations for direct implications in various fields such as wastewater treatment and sea-salt production and metal recycling.<sup>142</sup>

Other than the above-discussed SIWE devices, the performance of reduced GO is inevitable to avoid solar water

evaporation.<sup>76,143,144</sup> For instance, Xiong and his team investigated a reduced GO-based photothermal sheet with embedded hydroxyapatite nanowires (rGO/HNs) with high-efficiency SIWE and stable desalination.<sup>36</sup> Besides, the scalability and feasibility of the technology are the other essential characteristics of SIWE devices for an improved SIWE system. However, intrinsic barriers such as heat loss and insufficient water transport still prevail, preventing all of the prevailing designs from achieving the ultimate objective.

In an investigation by Fang *et al.*, activated carbon/fiber cloth with a matching water supply and durable fouling



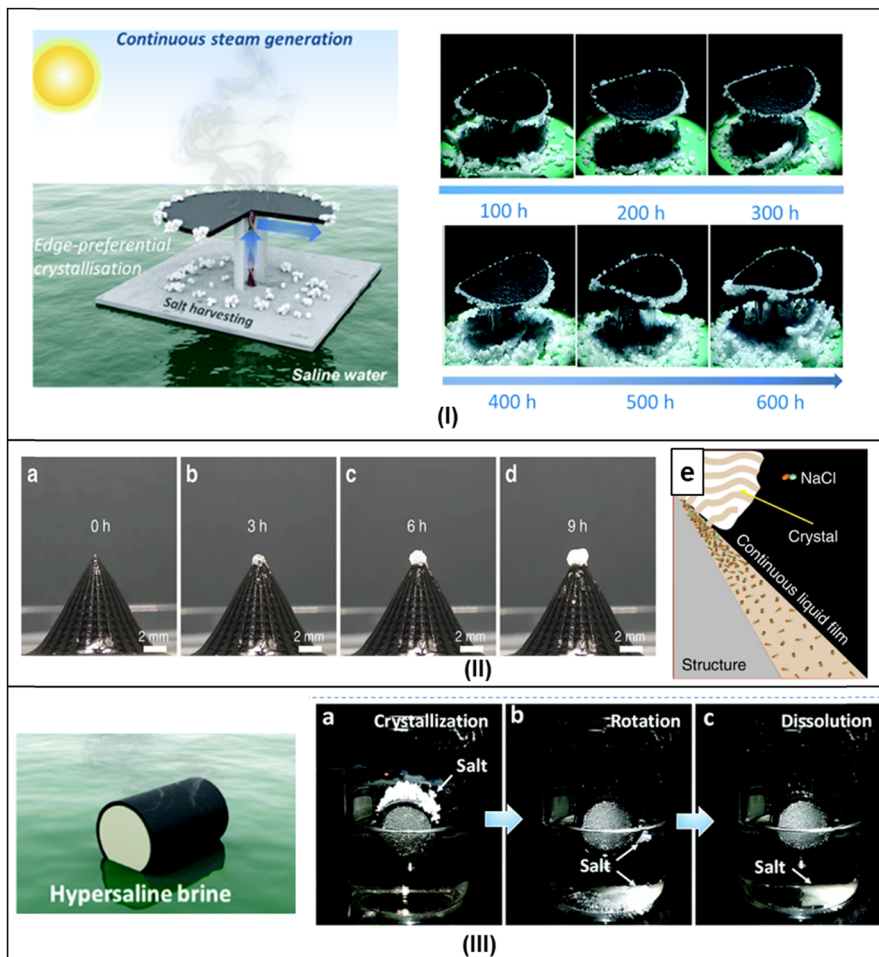


**Fig. 11** (I) Edge preferential salt crystallization; schematic design and virtual salt crystallization and collection. Reproduced with permission.<sup>109</sup> Copyright 2019, Royal Society of Chemistry. (II) Localized salt crystallization/salt harvesting; biomimetic 3D absorber; (a–d) time sequence of optical captures displaying the localized crystallization process on the biomimetic 3D evaporator and (e) scheme of the continuous water film along the sidewall of the evaporator that extends to the localized crystal at the apex position. Reproduced with permission.<sup>80</sup> Copyright 2020, Nature. (III) Self-rotating CNTs-based solar evaporator; schematic illustration and self-rotating mechanism (a–c). Reproduced with permission.<sup>141</sup> Copyright 2020, Royal Society of Chemistry.

resistance represented an excellent device with 93.3% efficiency and has great potential applications in solar desalination.<sup>145</sup> The study revealed that the balance maintained between the water supply and vapor evaporation is more important in fulfilling heat exploitation and effective solar desalination. Furthermore, the scalability and stability can be more justified with the use of a flexible and salt-resistive Janus absorber, either lotus-inspired<sup>104</sup> or a sunflower-inspired design (CB/PMMA/PAN).<sup>103</sup>

Although various reports have been studied to date, none provided an appropriate explanation of the stability and reusability of the system for a longer duration (Table 1).

Besides, very few talked about the actual practical issues of the proposed system, primarily the salt generation over time. This accumulation of salt over the evaporating surface arises due to salt nucleation and growth during solar evaporation as the concentration of water feed increases. This phenomenon hinders the continuous dynamic functioning of the device by

obstructing the water supply and reducing the absorption capability of the solar absorber.<sup>150</sup> Ideal solar desalination could be observed as a continuously operating system with high efficiency and no significant change in water evaporating rate over time. But to maintain this, appropriately directed salt-rejection strategies are needed<sup>151</sup> and they are: (i) natural dissolution and physical removal, (ii) enhanced fluid convection, (iii) hydrophobic-hydrophilic (Janus) design, and (iv) site-specific salt formation. The best method for removing salts is through physical cleanings, such as rinsing or washing. This method works best for flexible SIWE devices as they are simple to clean and require less intervention than bulk materials. Furthermore, for a stable SIWE operation, the natural dissolution of salt back to the seawater under the driving concentration gradient in the dark is a feasible solution. However, the above two strategies are traditional ways of salt rejection but include operational time constraints. To successfully perform these strategies, one requires a low-salinity brine as the water



**Table 1** Water evaporation and desalination performance based on different materials, under different light intensities, solar water evaporation efficiency and desalination efficiency along with stability and scalability

Materials	SIWE efficiency/ Light water evaporation rate	Light intensity ( $\text{kW m}^{-2}$ )	Desalination efficiency	Stability	Scalability	Ref.
Plasmonic-based SIWE devices	3D self-assembly Al NP/AAM structure	88%	4	4-order salinity decrements	Stable performance over 20 cycles (1 h per cycle)	Scalable 8
	Plasmonic Au NP/rGO aerogel	90.10%	1		Excellent stability with 120 h continuous operation	146
Polymer-based SIWE devices	HfN-AAO membrane	87%	1	3-order salinity decrements	Up to 10 cycles in freshwater	117
	Ultralight biomass PPY-coated porous foam	94.70%	1	Reduced ion concentration (salinity > 20 wt%)	30 days continuous operation	120
Semiconductor-based SIWE devices	PPY-coated VMP monolith foam	88%	1	Primary ion concentration dropped by one order magnitude	Good stability with salt resistance properties for more than 6 hours	121
	Nanocaged black titania	71%	1	Metal ions are largely reduced up to the permissible limits	Stable over more than 10 cycles	147
Hierarchical micro-structures of copper phosphate	Moth-eye-like nanostructured black titania	94%	1	With reduced metal ions concentration, 96% of rhodamine B is degraded	Stability, > 14 cycles	46
	Hierarchical micro-structures of copper phosphate	63.30%	1	For salinity 3.5 wt%, 1.13–1.85 $\text{kg m}^{-2} \text{h}^{-1}$ water evaporation was recorded	Stability > 6 cycles	15
CuO nanowire mesh	CuS/bacterial cellulose gel membrane	84.40%	1	58% of TOC removal	5 cycles of continuous operation	130
	Donan effect-based solar evaporator	98.50%	1	Reduced ions as per the permissible limits	Durable for more than 40 cycles, flexible, and effective salt resistance	Scalable 131
GO/PS foam	80% $\approx 1.3 \text{ kg m}^{-2} \text{h}^{-1}$	1	Decrement in four orders of magnitude	Stability up to 11 cycle continuous test treating a 15 wt% NaCl solution	148	
	80%		Four order salinity decrements	High stability over 10 cycles (each cycle per 1 hour)	Scalable 149	
Hierarchical graphene foam (h-G foam)	91.40%	1	Reduced ion concentration was recorded	Over continuous 20 cycles	12	
	Anti-clogging solar desalinator	62.70%	1	Five orders of desalination under high salinity	Showed stability over more than 5 hours of continuous operation	108
Self-rotating CNTs-based solar evaporator	1.41 $\text{kg m}^{-2} \text{h}^{-1}$	1	Five to six orders in magnitude under hypersaline brine (300 g $\text{L}^{-1}$ NaCl)	Stability around 30 days with continuous operation	141	
	CB NPs/Al <sub>2</sub> O <sub>3</sub> /copper foam	80%	1	Reduced ion concentration, meeting WHO standards	Operated for more than continuous 8 hours	142

feed and an optimized porous material balancing out the thermal and salt transfer efficiency to achieve efficient and long-run solar desalination with zero-crystalline salt formation. Similar strategies were demonstrated by various researchers, including Zhu *et al.*,<sup>82</sup> Ni *et al.*,<sup>152</sup> and Chen *et al.*<sup>153</sup>

Another advanced design is termed Janus, an intelligible hydrophobic/hydrophilic designed membrane for solar water evaporation. It includes a composite of two layers, the top hydrophobic layer for solar absorption and the bottom hydrophilic layer for water transport. With heat localization in the hydrophobic layer and water pumping in the hydrophilic layer, the device's heterogeneous wettability enables it to float on the water surface. As a result, the hydrophilic layer is the only place where salt ion concentration and nucleation take place. Although if the formed salt crystal is visible in this layer, it can still be gradually dissolved by water pumping. Similar phenomena are claimed by Xu *et al.*,<sup>103</sup> Yang *et al.*,<sup>154</sup> and Hu *et al.*<sup>155</sup> Despite being able to function at high salinity, the

Janus structure still struggles in terms of stability and durability of the hydrophobic coating in brine.

Besides the advancement of SIWE device design, the choice of materials having intrinsic self-generation capability is a favorable factor that should be taken into consideration for long-term SIWE device durability in brine. This quality allows solar evaporators to operate continuously without salt accumulation on the heating surface. This works on an enhanced fluid convection mechanism between the solar evaporator and the water reservoir, which can dilute the high-concentration brine within the evaporating area before the precipitation of salt crystals occurs. Along with speeding up the salt exchange to prevent the formation of hypersaline water, the rapid water flow encountered here also removes heat from the evaporation surface, further reducing conductivity loss. In response to this, Chen *et al.* introduced a unique method that maintains excellent heat localization, while spontaneously rejecting salt *via* improved fluid convection.<sup>152</sup> Nonetheless, the lack of



**Table 2** Water evaporation and desalination performance of SIWE devices based on hybrid materials under different light intensities, including solar water evaporation efficiency along with desalination efficiency

Materials	Substrate	Water purification efficiency (%)	Desalination efficiency	Light intensity ( $\text{kW m}^{-2}$ )	Ref.
Molybdenum carbide/carbon-based chitosan hydrogel	—	96.15	—	1 sun	18
Carbon nanotubes/Ni foam decorated with $\text{Fe}_2\text{O}_3$ nanoparticles	Ni foam	83.1	—	1 sun	157
CNTs@PVP photothermal membrane	Polystyrene	91.1	—	1 sun	158
AgNPs@ $\text{C}_3\text{N}_4$ /GO membrane	GO	77	—	1 sun	144
Ag/Au-GO-PU foam	Polyurethane	98.6	—	8 sun	77
$\text{Ti}_2\text{O}_3$ -PVA/LASH networking	Hydrogel	90	99.9%	1 sun	159
Cauliflower-shaped hierarchical copper nanostructures	Copper	60	—	1 sun	160
Nature-inspired, 3D origami solar steam generator	Cellulose	100	—	1 sun	161
Vertically aligned Janus MXene-based aerogels	PTFE	87	—	1 sun	47
Polydopamine-filled bacterial nanocellulose	BNC	78	—	1 sun	162
Stac nickel-cobalt@polydopamine nanosheet	Commercial sponge	109	Salinity up to 2.26 ppm	1 sun	156

knowledge regarding the behavior of water transport and the mechanism of salt rejection represents a setback for researchers.

Among the strategies, controlling the salt at a designated location or, in other words, the on-site salt formation offers a new and facile approach to the current heavy use of energy and cost within, providing a separate collection of fresh water and salt crystals without hampering the continuous operation for a more extended time. The movement of salt ions from a water source to a particular location, such as the edges of solar absorbers, is mostly fueled by capillary force. Water loss across the evaporative area causes the solute concentration to rise as the water flux gets closer to the endpoint. Due to the directional water flow, it is interesting to note that salt crystallization only occurs at the terminal site, leaving the majority of the solar evaporators free from the salt problem. In addition to efficiently extracting salt from brine, this modified salt distribution can support water evaporation.<sup>151</sup> A recent report by Wang *et al.* fabricated a 3D-shaped cup to achieve ZLD desalination with high energy efficiency *via* solar water evaporation. Compared with the similar conventional 2D design and 3D design, the latter proved to be the most effective in a highly harsh salt environment (25 wt%), without any conspicuous change in water evaporation rate for at least 120 h.<sup>80</sup> Interestingly, Xia *et al.* reported a solar steam generator (CNTs/filter paper/polystyrene foam) that could achieve continuous steam generation and salt harvesting in an uninterrupted long run over 600 h (Fig. 11(I)). The evaporation strategy of salt solution transport and distribution over the photothermal material in the form of discs having one inlet, two inlets, and four inlets quickly controlled the deposition. The proposed design successfully achieved the spatial isolation of salt crystallization from water evaporation and advanced one more step further toward practical applications of solar steam technology, demonstrating great potential in seawater desalination and resource recovery from wastewater with zero liquid discharge and in-hand salt harvesting.<sup>109</sup> Likewise, Wu *et al.* developed a biomimetic 3D absorber, where the crystallized salt stands freely on the evaporator and can be easily removed (as shown in Fig. 11(II)). The system achieved a water evaporation rate of

2.63  $\text{kg m}^{-2} \text{ h}^{-1}$ , with energy efficiency exceeding 96% under one sun illumination. Furthermore, in a closed system and under high salinity (25 wt% NaCl) of natural seawater, the water collected at a rate of 1.72  $\text{kg m}^{-2} \text{ h}^{-1}$ .<sup>80</sup> In addition, it is necessary to note that salt accumulation has a negligible impact on energy efficiency and water evaporation of the system, indicating the potentiality of the novel strategy for sustainable and practical applications in the future.

**3.1.5 Composite-based SIWE devices.** Apart from the individual functionalities of the solar absorbers, the combination of these plays a vital role in SWIE-enhanced functioning. For instance, Shao *et al.* presented an energy conversion efficiency of about 109% using the  $\text{Ni}_1\text{Co}_3$ @PDA-based photothermal sponge.<sup>156</sup> Likewise, the arrangement of CNTs and GO over the low conductive substrate demonstrated a conversion energy efficiency close to 100% with optical absorption of more than 97%. With this, there are other studies as well exhibiting a similar impression (Table 2).

### 3.2 Energy generation

Under the basic functioning of SIWE, an inevitable amount of heat is lost to the surroundings. On the contrary to this energy loss, electricity production applications have found an opportunity in a hybrid form to solve the water and energy insufficiency simultaneously. A few researchers have fruitfully used this concept to perform more effective thermal management of SIWE systems. This can be done through the integration of different electricity generation strategies, including salinity gradient power, thermoelectric conversion, photovoltaics (PVs), and thermogalvanic cells. Despite all the solar absorbers having potential, carbon-based SIWE is one that has received a lot of research attention when it comes to the type of solar absorber utilization, particularly for simultaneous electricity generation. For instance, a report published by Zhu *et al.* successfully demonstrated one-site electricity generation and freshwater production in one go. They introduced a 3D elastic cellular nitrogen-enriched carbon sponge (CS), as an indeed proposed SIWE device with an induced electrical potential and  $2.4 \times 10^{-5}\%$  solar-electric conversion efficiency.<sup>163</sup> They were the first to demonstrate the SWIE-induced electric potential.





Table 3 Electricity generation performance of SIWE devices under different light intensities, solar water evaporation efficiency, power generation, stability, and scalability

	Materials	Carrier	SIWE efficiency/water evaporation rate	Power generation	Light intensity	Stability	Scalability	Ref.
Plasmonic-based SIWE devices	AuFs	Silica hydrogel	85%	0.63 $\mu\text{W m}^{-2}$	1	Reusable and recyclable	Scalable	168
	Polydopamine nanofibrils	Sodium alginate 2.56 kg m <sup>-2</sup> h <sup>-1</sup> aerogel	5.6%	1				169
Polymer-based SIWE devices	Monolithic carbon sponge	90%	$V_{\text{OC}} = -80 \text{ nA}, I_{\text{SC}} = 1 -20 \text{ V}$	1			Scalable	163
	Carbon nanotube-modified filter paper Naion membrane	75%	12.5 W m <sup>-2</sup>	1	20 h	Stable performance for Scalable	Scalable	166
Carbon-based SIWE devices	Non-woven film	82%	292.9 W m <sup>-2</sup> (4.17 V & 0.6 A)	30			Scalable	115
	Nickel foam	87.20%	0.175 W m <sup>-2</sup>	1		Mechanically stable, flexible, and recyclable		24
Carbon	$\text{Bi}_2\text{Te}_3$ -based TEG	1.36 kg m <sup>-2</sup> h <sup>-1</sup>	0.4 W cm <sup>-2</sup>	1		Highly stable and robust for long-term use (8 h of a continuous cycle), extremely reliable, especially for rural and remote areas		170
	Graphene foil equipped with solar cell CNTs	Porous graphene sponge Cellulose paper	2.01–2.61 kg m <sup>-2</sup> h <sup>-1</sup>	0.20–0.37 kW m <sup>-2</sup>	1	$I = 22 \mu\text{A}$	Maintain a continuous current output over 6 hours	Fast and scalable for mass production Scalable
Hybrid-based SIWE device	Hydrogel/metal oxide/polymer-based multilayered PPCC cell	Hydrogel	1.33 kg m <sup>-2</sup> h <sup>-1</sup>	$\approx 1.6 \text{ mW m}^{-2}$	1 kW m <sup>-2</sup>	1 kW m <sup>-2</sup>	High mechanical stability along with resistance to diverse water environments, reusable and recyclable, as well	Scalable under different prototypes

For this, a ferroelectric fluoropolymer polyvinylidene fluoride (PVDF) film was used, which efficiently endures the simultaneous heating and cooling variation caused by the interaction of natural air flow and the generated steam. Reaching the PVDF film's surface, water vapor condenses in the form of numerous microscopic water droplets, which heats the PVDF film. The local humidity around the PVDF film drops as the vapor drifts away and the water droplets quickly evaporate, cooling the PVDF layer. Later an external load resistance is employed to measure the pyroelectric response of the film.

Apart from the pyroelectric energy generation, an induced salinity gradient can be noted in the case of water evaporation or desalination using plasmonic nanostructures, the other provision for electricity generation.<sup>164,165</sup> Similarly, Zhou *et al.* fabricated a self-floating hybrid system, having CNT-modified paper over an ion-selective membrane called Nafion. The device recorded a thermal efficiency of around 75% under one sun and an electrical output power of  $\sim 1 \text{ W m}^{-2}$  simultaneously and was later suggested to improve with some further optimizations.<sup>166</sup>

Interestingly, various attempts were made to balance the energy within the proposed system (Table 3). For instance, Zhu and his co-workers developed a solar-driven interfacial evaporation-thermoelectric-induced device using cost-effective, highly efficient, and scalable graphite particles coated over a non-woven material. Fig. 12(I) demonstrates the same for a sizeable real-scale application. The result was quite attractive, with a solar-thermal conversion efficiency of around 81.5%, meeting the WHO standards for drinking water. In addition, the system achieves maximum solar-electricity efficiency of 1.23% (4.17 V and 0.6 A).<sup>115</sup> Likewise, Ho *et al.* reported an evaporation rate of  $1.20 \text{ kg m}^{-2} \text{ h}^{-1}$ , an efficiency of 87.4%, and an output power density of  $0.063 \text{ W m}^{-2}$  under one sun irradiation, using a 3D organic sponge as a SIWE device.<sup>167</sup> Meanwhile, this group also creatively used a ferroelectric PVDF film to harvest the thermomechanical responses during solar evaporation, achieving the output power of  $240.7 \text{ } \mu\text{W m}^{-2}$ .<sup>163</sup>

Zhu *et al.* formulated a 3D organic sponge with the desired properties that render both the photothermal vaporization and electricity generation ability along with the enhanced operational durability (Fig. 12(III)). Under a realistic one sun scenario, the thermoelectric module functions as a heat insulator to enhance solar water evaporation and simultaneously harvests low-grade solar heat to sustain power.<sup>167</sup> Likewise, a monolithic design was proposed by Xiao *et al.*, using an asymmetric functionalization strategy successfully responding to this concept, enabling effective solar-thermal-electro integration in one system (Fig. 12(II)).<sup>173</sup>

Besides, Jiang *et al.* and his team proposed a universal solar water evaporation system that effectively distilled various water sources (seawater, river water, strong acid-alkali water, and organic dye wastewater) (as shown in Fig. 12(IV)).<sup>24</sup> The nickel sulfide/nickel foam-based solar evaporator is stated to have a water evaporation rate of about  $1.29 \text{ kg m}^{-2} \text{ h}^{-1}$  with a conversion efficiency of 87.2% under one sun irradiation. Using the same system with a thermoelectric (TE) module as an insulator,

a maximum power output of about  $0.175 \text{ W m}^{-2}$  was achieved. Henceforth, we can observe this heat management and integration of solar water evaporation systems with energy generation as an attractive footstep towards the era of one solution to various problems.

Moreover, Ding *et al.* presented an optimized integrated cross-flow multi-stage membrane distiller model and PV cell with an advanced latent heat recycling option.<sup>174</sup> The PV cell module above the distillation unit transports its waste energy to the bottom distillation unit to generate fresh water. The distillation unit is composed of an optimized hydrophobic membrane managing the thermal energy and a multi-stage membrane balancing vapor and heat transport. This results in higher electricity output and water yield. Similarly, Ji *et al.* presented a rational, integrated semitransparent PV cell and an interfacial steam generator (SG) producing a high electrical power output of  $122 \text{ W m}^{-2}$  and  $1.30 \text{ kg m}^{-2} \text{ h}^{-1}$  water evaporation rate simultaneously.<sup>175</sup>

Recently, Huang *et al.* anticipated a sustainable clean-water production and green-energy generation technology *via* GO nanosheets with different assemblies (1D aligned fibers, 2D layered membranes, and 3D porous foam). With the excellent chemical properties of GO, an efficiency of over 95% with water generation rates of  $2.0\text{--}2.4 \text{ kg m}^{-2} \text{ h}^{-1}$  under one sun irradiation was achieved. Under electricity generation, an increased magnitude from 30 mV to 1.5 V was observed in a single device *via* modulation of the chemical groups present and the moisture absorption capability. The fabricated device demonstrated a unique and promising approach to the water-energy nexus.<sup>176</sup> Recently, Sun *et al.* developed a novel, simple, bioinspired, multi-layered, and designed interfacial evaporation-driven nanogenerator (IENG). This multi-functional system includes a porous ionic hydrogel in the bottom for water feed, the middle layer is built of multi-walled carbon nanotubes, MXene is used to increase electric conductivity, and the top layer is constructed of nanofibers to generate heat and electricity. The IENG demonstrates an output power density of  $11.8 \text{ } \mu\text{W cm}^{-2}$ , which is 6.8 times greater than the previously documented average value with a high evaporation rate of  $2.78 \text{ kg m}^{-2} \text{ h}^{-1}$ .<sup>177</sup> Altogether, research on electricity generation has shown the potentiality of SIWE devices along with freshwater generation, but these contributions are still small for real-life practices because of their high cost and the techniques involved.

### 3.3 Wastewater evaporation

Apart from studying a highly efficient and endurable solar water evaporation system, this concept shows a variety of diverse applications. One is wastewater treatment – cleaning up heavy metal or ion contamination, micro-organisms, industrial effluents, *etc.*, from the water resource to make it fit for other basic needs.<sup>84,178</sup> With regard to the wastewater without volatile organic compounds (VOCs), SIWE's evaporation and condensation mechanism separates the clean water leaving behind the concentrated wastewater containing the pollutants.<sup>61</sup> For example, the superheated steam generated under ambient pressure and low-flux solar irradiation is an



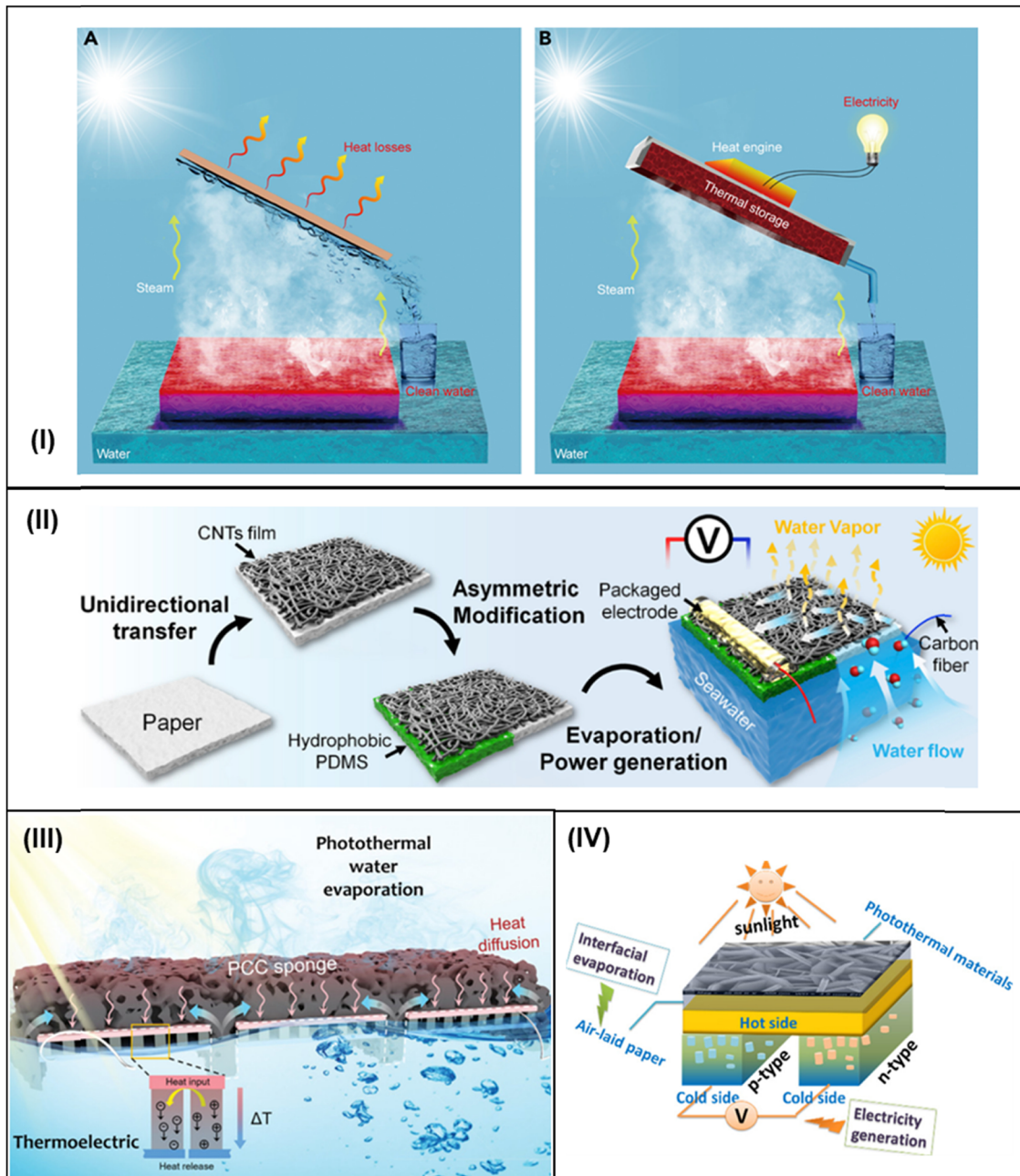


**Fig. 12** Electricity generation. (I) A multifunctional system, with clean water generation and electricity production simultaneously. Reproduced with permission.<sup>115</sup> Copyright 2018, Elsevier. (II) All-in-one evaporator to generate electricity through water flow during evaporation. Reproduced with permission.<sup>173</sup> Copyright 2020, Elsevier. (III) Schematic of the synergistic interfacial photothermal water evaporation and thermoelectricity generation process based on PCC sponge. Reproduced with permission.<sup>167</sup> Copyright 2019, Wiley-VCH. (IV) Schematic illustration of nickel sulfide/nickel foam-based solar evaporator demonstrating simultaneous clean water and electricity generation. Reproduced with permission.<sup>24</sup> Copyright 2020, American Chemical Society.

effective parameter in the removal of both the *Geobacillus stearothermophilus* biological indicator and *Escherichia coli* bacteria. Herein, the authors demonstrated a solar vacuum tube working under an interfacial evaporation mechanism, capable of generating steam above 121 °C in ambient fluctuating solar illumination with an averaged natural solar irradiation of ~600 W m<sup>-2</sup>. Moreover, as a steam generator, the vacuum tube achieves a temperature of about 102 to 165 °C and solar-to-

steam conversion efficiency from 26 to 49% under one sun illumination.<sup>179</sup>

Furthermore, inhibiting the enrichment of VOCs in the condensed water for wastewater containing VOCs is essential and is frequently accomplished using two techniques.<sup>180</sup> One includes the integration of advanced oxidation technologies.<sup>51</sup> In particular, with the direct implication of solar energy on eco-friendly wastewater treatment, Zhu and his co-workers

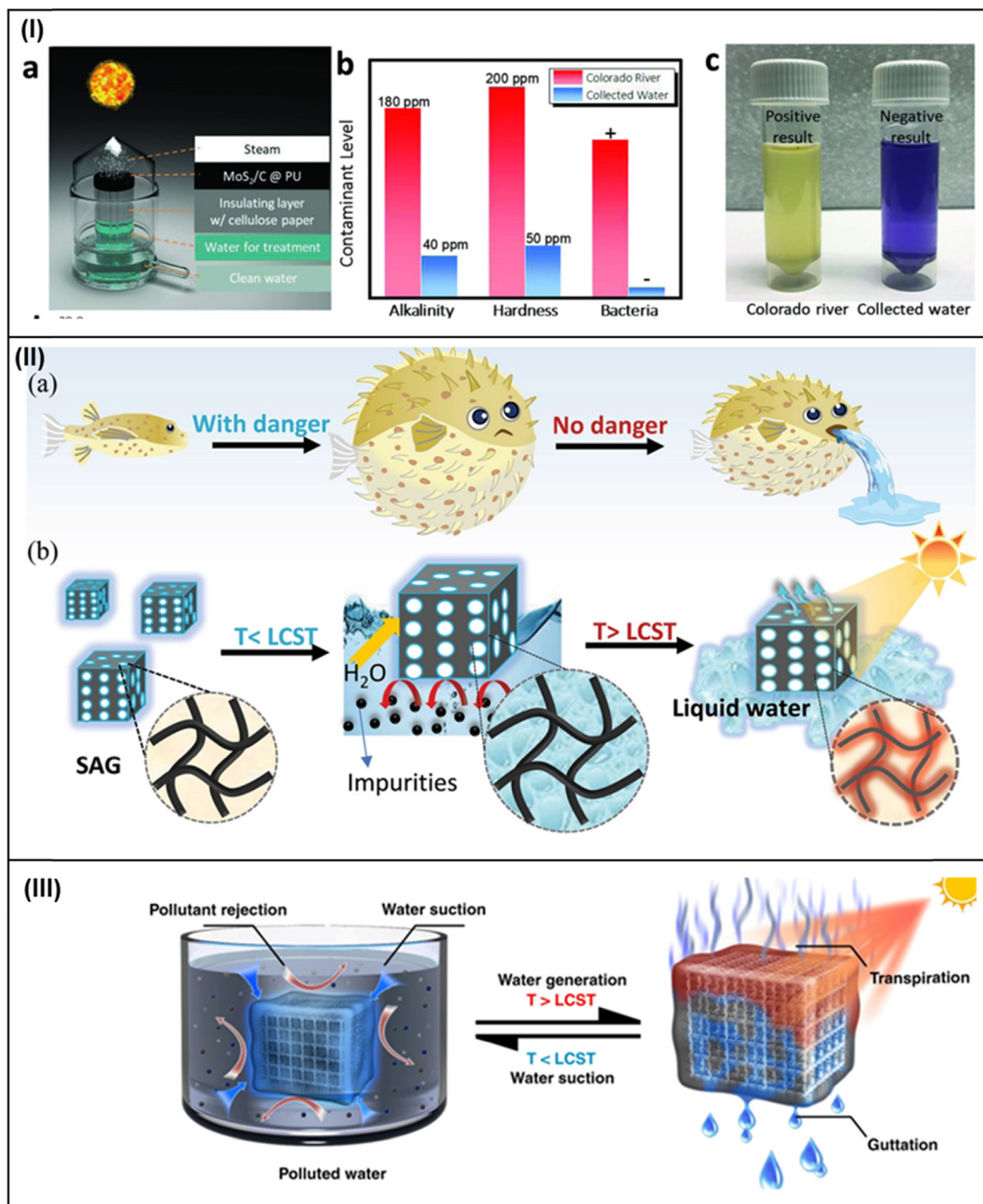


**Fig. 13** Wastewater purification via SIWE devices. (I) (a–c) MoS<sub>2</sub>/C@PU solar steamer – design and performance. Reproduced with permission.<sup>184</sup> Copyright 2018, Wiley-VCH. (II) Design illustration of a solar absorber gel for clean water production. Reproduced with permission.<sup>185</sup> Copyright 2021, Wiley-VCH. (III) Schematic of water treatment of the sunlight-powered purifier (PNPG-F) – the coated PG demonstrates solar–thermal conversion and pollutant rejection. Reproduced with permission.<sup>65</sup> Copyright 2019, Nature.

examined the performance of a tailored semiconductor-based photothermal sheet as the SIWE device, providing more photocatalytic active sites and longer reaction distances.<sup>181</sup> The study depicted the concentrations of heavy metals such as Cu<sup>2+</sup>, Cr<sup>3+</sup>, and Pb<sup>2+</sup> as much lower than the concentrations found in effluents. In addition, the decreased concentration of Rhodamine B dye from 10<sup>-5</sup> mol L<sup>-1</sup> to 10<sup>-11</sup> mol L<sup>-1</sup> was recorded as well. Similarly, a few researchers have reported almost a complete discoloration of organic pigments – methyl orange, methyl blue, and colored heavy metals as well as the

inactivation of pathogens polluting the water environment.<sup>154,182,183</sup> Added to these, a study led by Li *et al.* demonstrated a high evaporation rate of 1.95 kg m<sup>-2</sup> h<sup>-1</sup> under one sun intensity and showed water treatment facilities, particularly for the Hg<sup>+</sup> ion from 200 to its permissible limit of ~1 ppb, *via* a MoS<sub>2</sub>/C-based PU composite sponge, as the SIWE device (Fig. 13(I)).<sup>184</sup> Moreover, a recent report submitted by Tian *et al.* practically examined the as-designed evaporation system for multiple wastewater evaporation, such as, the wastewater coming from dye pollution, micro-organism pollution, and



**Table 4** Wastewater purification performance of SIWE devices under different light intensities, solar water evaporation efficiency, pollutant concentration after purification, long-term stability, and scalability

Materials	SWE efficiency/ water evapora- tion rate	Light intensity (kW m <sup>-2</sup> )	Comments	Stability	Scalability	Ref.
Hydrophobic Cu <sub>2</sub> SnSe <sub>3</sub> nanosphere array	86.60%	1	Reduction beyond 99.5%	Excellent stability over a continuous period of 15 days	Scalable	154
Biochar-material-based solar absorber	80.00%	1	≈99.99% degradation of all targeted bacteria	Outstanding stability with a short sterilization period	Scalable	188
Carbon-molybdenum-disulfide microbeads over PU	88%	1	99.6% degradation of Hg ions	—	Scalable	184
Organic CT (charge transfer) complexes	90%		~99.9% reduction was recorded	Shows stability over 8 hours of continuous operation	Scalable	25
Self-assembled asymmetric Ag plasmonic structure	80%	4	20% decay on-site	Durable performance up to 45 days	Scalable	187
Poly( <i>N</i> -isopropylacrylamide) hydrogel	4.2 kg m <sup>-2</sup> h <sup>-1</sup>	1	~99% reduction in pollutant	Long-term use	Scalable and modular	185
Photo-responsive solar absorber gel	7.18 kg m <sup>-2</sup> h <sup>-1</sup>	1	Decontaminates various dye molecules, heavy metals, oil, and yeast	Stable up to 10 cycles with impressive inherited properties	Scalable and modular	185
Fe-MOF hybrid hydrogel	90% 3.2 kg m <sup>-2</sup> h <sup>-1</sup>	1	Applicable for high salinity and various metal ions reduced to 4–7 orders of magnitude over 2 h of operation	Long-term desalination with no additional post-treatments	Scalable with high potential	189
TiO <sub>2</sub> -PDA/PPy/cotton D-HNb <sub>3</sub> O <sub>8</sub> /PAM aerogel	1.55 kg m <sup>-2</sup> h <sup>-1</sup> 1.401 kg m <sup>-2</sup> h <sup>-1</sup>	1	96% degradation of MO after 3 h 70% RhB within 100 min (UV-vis irradiation)	Stable up to 7 cycles with no functional deterioration, suggested to be mechanically durable and recyclable	Scalable and could be used as a portable solution	192
CB-based nano ink-stained PVA sponge 3D hierarchical solar vapor generator (3DHG) CNT/wood-PVA	96.48%, 2.15 kg m <sup>-2</sup> h <sup>-1</sup> 98.1%, 1.56 kg m <sup>-2</sup> h <sup>-1</sup> ~96.9%	1	Affable approach to mixed dyes and domestic wastewater The dissolved salts get reduced by 3–5 orders of their Novel approach, stable up to 7 days under continuous operation	Good durability	Not reliable for strong illumination	193
Self-channelled, multi-functional photothermal sand system Cu <sub>x</sub> S/Cu foam (SCF) evaporator	1.43 kg m <sup>-2</sup> h <sup>-1</sup> 94.5%, 1.96 kg m <sup>-2</sup> h <sup>-1</sup>	1	99.7% purification efficiency esp. for the waste oil contents Concentrations of ions recorded were far below the WHO standards, sustainable purification was observed for oil-spillage 0.23 kg m <sup>-2</sup> h <sup>-1</sup> water evaporation rate for oil–water emulsion and ion concentrations below the WHO standards	Stability up to continuous 15 cycles and durability till 7 successive days of evaporation	Highly scalable with advanced results (even for an invisible water source)	195
				Long-term stability for 50 h of operation	Scalable, with remarkable consecutive outdoor test	196

heavy metal pollution, besides the basic functioning of SIWE devices. The system ultimately noted high water evaporation efficiency of 99.8%, meeting the WHO standards of potable water.<sup>25</sup>

Additionally, the second approach of wastewater cleaning relies on physical interception and involves the separation of water and VOCs based on the various solution diffusion behaviors of water and VOCs within polymeric membranes.<sup>186</sup> These membranes can filter out complicated volatile organic pollutants from natural water sources and provide water that complies with drinking water standards. For example, Chen *et al.* and his team tested the developed SIWE device's durability in a harsh wastewater environment. A dual functional APS (asymmetric plasmonic structure) of Ag NPs based SIWE device enabled on-site pollution detection and purification of water simultaneously, exhibiting prolonged durability for 45 days under natural sunlight conditions.<sup>187</sup> A recent study published by a group of researchers on the successful development of a solar absorber gel, showed eliminating the need to heat and evaporate water altogether. Taking inspiration from the pufferfish's ability to inflate and deflate itself with water in response to danger, but in this case, absorbing contaminated water and spitting out clean drinking water (Fig. 13(II)). Polydopamine (PDA), a polymer derived from melanin, which shows broadband solar absorption and light conversion efficiency, was utilized in the current work by the team. As a result, they developed a hydrogel that releases the water it absorbed when warmed by sunlight.<sup>185</sup> Recently, Geng *et al.* demonstrated a plant leaf water purifier.<sup>65</sup> As shown in Fig. 13(III), they constructed a poly(*N*-isopropyl acrylamide) hydrogel (PN) attached to a super hydrophilic melamine foam skeleton, along with an outside coated layer of PNIPAm-modified graphene (PG) filter membrane. This coherent engineered structure reported a high ion rejection capability of >90%, with a water collection rate of  $4.2 \text{ kg m}^{-2} \text{ h}^{-1}$  from the contaminated water source. Table 4 incorporates a few more research studies with a distinctive approach. Although these reports broach the feasible, eco-friendly, and low-energy utilization nature of this application, the stable functioning of the system under a complex wastewater environment, the adsorption and removal of dyes and metal ions over the evaporating surface are still challenging and concerning parameters, similar to that discussed for salt accumulation. In addition, deep research is essential on the components' separation order, separation speed, and separation time for smooth operation.

### 3.4 Other applications

Besides water processing, purification or treatment and real-time electricity generation, solar-driven water evaporation works well under the scheme of public health and medical needs, dropping out the excess electricity requirement such as in steam sterilization<sup>113,197</sup> and others, for the production of beneficial compounds and their by-products.<sup>198,199</sup> Deng and his team produced a highly promising, affordable solar water evaporator device, meeting the requirements of steam sterilization based on interfacial heating. The system includes a self-

floating rGO-based SWE device, enabling steam production at temperatures above 120 °C.<sup>113</sup> In a similar context, Chang *et al.* presented a highly efficient portable solar vacuum tube generating supersaturated steam with sterilization hold against *Escherichia coli* bacteria under ambient pressure and low solar flux (Fig. 14(I)).<sup>179</sup> By virtue of the dearth of readily accessible sterilizing methods in medical settings, Oara *et al.* fabricated two compact solar steam sterilization systems with open and closed-loop solar autoclave systems, generating steam using broadband, super light-absorbing nanoparticles. The systems maintain temperatures between 115 °C and 132 °C, with a capacity of 14.2 L.<sup>197</sup>

A study led by Grime *et al.* demonstrated the successful conversion of harmful gases into beneficial hydrocarbon fuels. The research utilizes the photocatalytic phenomena *via* nitrogen-doped titanium dioxide photocatalysts in the form of nanotube arrays under the assistance of solar irradiation. The device reported tremendous results, being capable of producing hydrocarbons at the rate of 111 ppm  $\text{cm}^{-2} \text{ h}^{-1}$ .<sup>111</sup> Besides these, the concept works well in the petroleum extraction processes to reduce the wax deposition over the pipelines. Chang and his co-workers formulated a 3D solar interfacial evaporator, whose steam generation is utilized to heat up the copper pipeline, thereby collecting deposited paraffin into the container (Fig. 14(II)).<sup>200</sup> Research also suggested the concept of utilization in waste sterilization and liquid separation, mainly in low-responsive areas.<sup>199</sup>

De-icing, a crucial new technique based on the SIWE process, is nevertheless significant despite the other mentioned applications. High light-to-heat conversion efficiency, quick heat transport throughout the surface, and minimal transverse heat loss are anticipated characteristics of the ideal photothermal de-icing surface. Wang's team used a modified templating approach to create a PDMS/rGO surface with a hierarchical structure. The light was absorbed from 295 to 2500 nm due to macropores and micro wrinkles (Fig. 14(III)).<sup>201</sup> They could function even at 60 °C, attributed to the remarkable photothermal efficient coating (>90%). Likewise, Dash *et al.* proposed a multi-layered de-icing coating capable of restricting the surface temperature to as high as 33 °C under ambient solar flux.<sup>112</sup> Other reported articles include the research of Cheng *et al.*,<sup>202</sup> Jiang *et al.*,<sup>203</sup> etc.

## 4. Progress and challenges in making facilities (real-life use) for different applications

Solar evaporation has emerged as a facile and attractive technology for clean water production, desalination, wastewater treatment, energy generation, *etc.*, as shown in earlier sections. However, the unsuccessful amalgamation of these hybrids and complicated solar-thermal devices with poor material compliance undermines extensive solar energy utilization and practical outdoor uses. Some practical experiences observed are listed



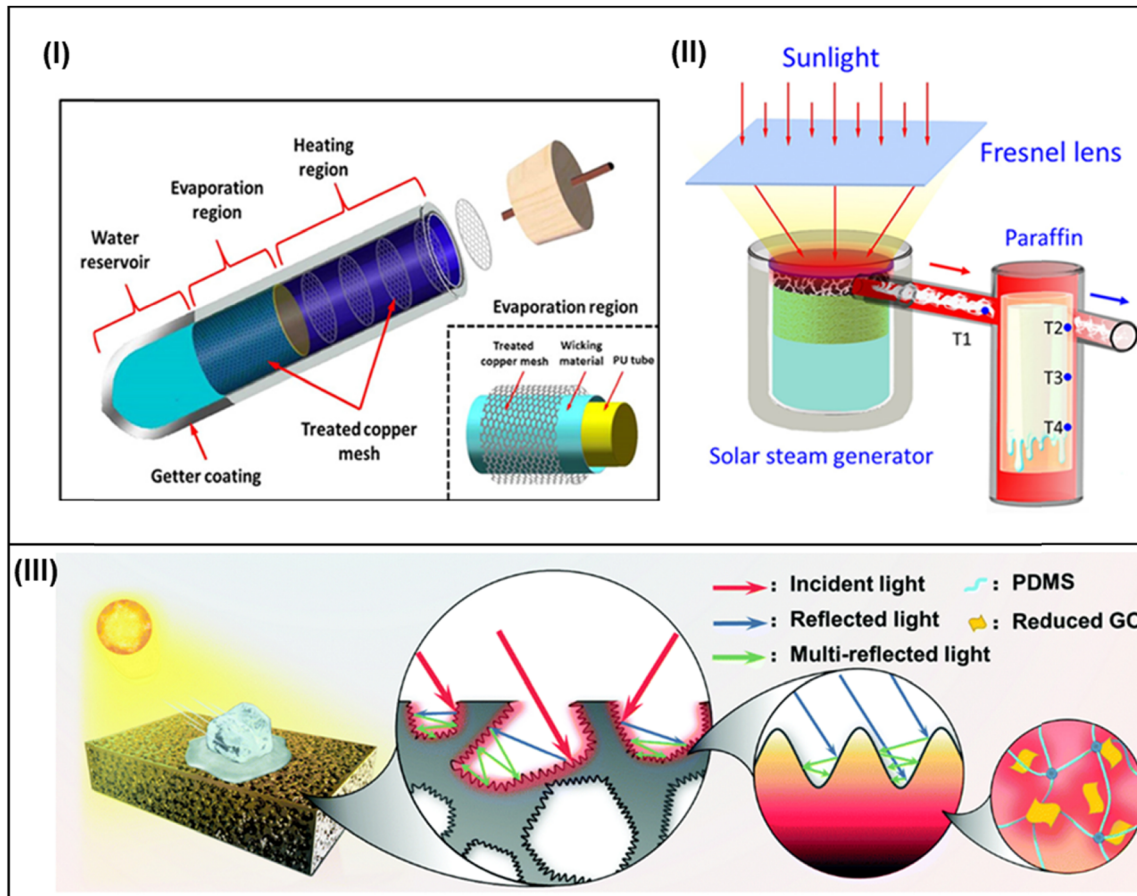


Fig. 14 Other potential applications of SIWE devices. (I) A portable solar steam generator. Reproduced with permission.<sup>179</sup> Copyright 2019, American Chemical Society. (II) Schematic setup for outdoor removal of paraffin deposits on the walls of oil pipelines. Reproduced with permission.<sup>200</sup> Copyright 2019, American Chemical Society. (III) A photothermal active deicing device performance. Reproduced with permission.<sup>201</sup> Copyright 2020, Royal Society of Chemistry.

in this section, underlining the real-life exposure and the real challenges faced.

To begin, Zhang and his team strategized a self-healing hydrophobic photothermal membrane based on PPy onto a SS mesh for large-scale fabrication, with the potential of portable water generation. Generally, a solar water evaporation system comprises an insulated chamber with a single transparent and tilted rooftop. The solar absorber is placed at the bottom of the chamber, and the whole solar distillation device floats on water. Zhang *et al.* fabricated a similar device consisting of an evaporating and condensing chamber separated by a division in the bottom. The solar absorber at the bottom functions accordingly upon solar irradiation and evaporation occurs. This system also includes a solar-powered fan for constant airflow inside the chamber, thus providing a way to collect water from the evaporation chamber to the condensing bottom at a rate of  $0.15 \text{ kg m}^{-2} \text{ h}^{-1}$ . But as the device failed to mention the input solar irradiation to the system, its capability to purify water cannot be fully appraised. Moreover, the device recorded lower evaporation efficiency, while functioning based on the distributed heating phenomena. Also, when referring to

its commercialization, the work failed to explain the device's stability, scalability, and cost-effectiveness.<sup>60</sup>

Later, a group of researchers fabricated a similar design based on localized heating to have higher outcomes (Fig. 15(I)). There, they formulated a small-sized graphene oxide aerogel (srGA) photothermal sheet having an area of around  $750 \text{ cm}^2$  over the lake in the form of a floating type solar still to measure the water productivity under ambient outdoor conditions. The entire floating device was a 3D thermally insulated tank made of PS with hydrophilic cotton bar wicks attached to the absorber through the substrate beneath. The design demonstrated water productivity of  $9.52 \text{ L m}^{-2} \text{ day}^{-1}$  under natural solar intensity, which could sufficiently cover the daily water requirement for five people. Other than these, 99.2% of heavy metal ion rejection was observed with the design stability of 10 cycles (6 h each). With excellent results, the device could be a promising solution for seawater, wastewater, sewage, *etc.* but is still hindered by the stability and recyclability of the system.<sup>204</sup>

Unlike the above-described systems, a low-cost and salt-rejecting floating solar still has been proposed by Ni *et al.*,

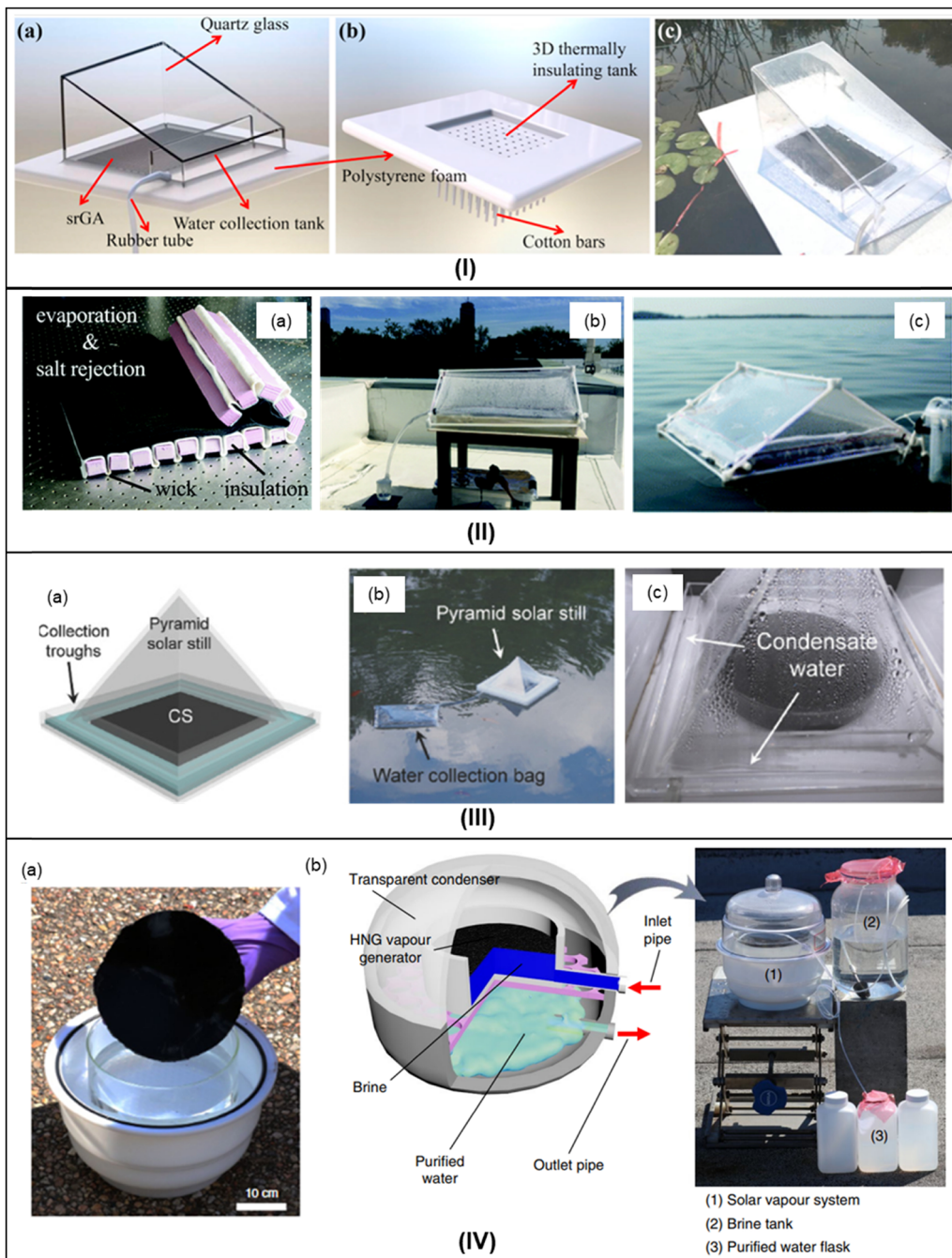


**Fig. 15** (I) (a) The scheme of the lab-made solar still. (b) The entire device floating on the lake, and (c) a virtual view of the solar still placed on outdoor water. Reproduced with permission.<sup>204</sup> Copyright 2018, Elsevier. (II) (a) Photograph of the evaporation structure, (b) rooftop experiments with the floating solar still under natural sunlight, and (c) testing of the floating still on the coast of the Atlantic Ocean. Reproduced with permission.<sup>152</sup> Copyright 2018, Royal Society of Chemistry. (III) (a and b) Schematic diagrams and photographs of the pyramid solar still floating on water and (c) the photograph of condensate water in the troughs of the pyramid solar still. Reproduced with permission.<sup>163</sup> Copyright 2018, Wiley-VCH and (IV) (a-c) outdoor solar water purification using HNGs under natural sunlight. Reproduced with permission.<sup>10</sup> Copyright 2018, Nature.

stating the conceptual interfacial heat localization as effectual desalination. They used porous and hydrophilic white fabric to wick water to the solar-absorbing evaporation structure above, while assuming advection and diffusion as the phenomena pushing the salt down to its previous position (as shown in Fig. 15(II)). The design (55 cm × 55 cm) modulated a dual-slope

structure entirely based on polymeric and fabric materials, generating pure water (50 ppm) at a rate of  $2.5 \text{ L m}^{-2} \text{ day}^{-1}$ . Economically, the entire system's material cost was  $\$3 \text{ m}^2$ , much lower than those of the conventional solar stills, without any additional energy requirement, providing cheap drinking water to water-stressed and disaster-stricken communities.

Finally, upon ocean testing, the effectiveness was comparatively lower than the rooftop, limiting the conduction loss beneath the substrate and having additional convection losses within the ocean currents. Furthermore, the device suffered from a transmission loss of about 20%, reducing the evaporation efficiency of the system. Hence, although the design provided simple and cost effectual fabrication, the challenges over the structural design, material choice, stability, and little understanding of the salt coagulation over the evaporating surface still prevail and need to be resolved when it comes to the real-life exposure.<sup>152</sup>

With the advancement in design, Ho and his team assembled a pyramid solar distillation cell to capture more and more sunlight throughout the day and validate water purification under natural ambient conditions. As shown in Fig. 15(III), the pyramid model consists of transparent, low-density acrylic boards with a carbon sponge (CS) as the solar absorber, assembled such that the water condenses at the collection troughs and then at the water collecting bag. The study reported a maximum freshwater generation of  $0.34 \text{ kg m}^{-2} \text{ h}^{-1}$  under one sun illumination. However, without a water collector, the water evaporation rate was observed to be  $1.15 \text{ kg m}^{-2} \text{ h}^{-1}$ , three times higher than that of the system with the water collection provision. The researchers noticed the difference and concluded that the humidity factor plays a significant role inside the sealed chamber; that is, the more the humidity, the lower the efficiency recorded. Furthermore, when the vapor condenses on the cover, the resultant water droplets condense on the transparent cover, blocking the incident rays and deteriorating the system's overall performance. Hence, structural design, material selection, and proper integration must be considered to simultaneously accelerate the rapid evaporation process and water collection.<sup>163</sup>

With the experience from the earlier made designs, adding a reflective layer to the absorber resulted in a relative increase in absorption efficiency by 6.5% and water evaporation efficiency by 12.2% compared to the system without this addition. Fan *et al.* and his team proposed this, claiming their evaporator to be an ideal candidate for scalable, practical applications with advantages of facile fabrication, durability, high cost-efficiency, and a good resistivity towards salt accumulation over time. To have a real-life experience, a portable outdoor prototype was designed, costing around  $30\text{S\$ m}^{-2}$  with an area of about  $1 \text{ m}^2$ .<sup>205</sup> Similarly, various researchers have successfully demonstrated the outdoor practical applications of their designed evaporators with average water.<sup>10,62,131</sup> For instance, Fig. 15(IV) presents a floating HNG-based water evaporator with a higher water evaporation rate of  $3.2 \text{ kg m}^{-2} \text{ h}^{-1}$  via 94% solar energy under one sun irradiation. Besides the laboratory scale investigation, Zhao *et al.* studied the outdoor vapor generation under natural conditions and reported collecting 18–23 litres of water per square meter of HNG, daily purifying seawater.<sup>10</sup> All these designs pave the way for various real-world applications in the future but are still underrated.

Forging ahead, conceptually utilizing the interfacial solar heat localization and vaporization enthalpy and recycling, the

multistage device's proposal enlightens the SIWE system's energetic performance. Here, Wang *et al.* demonstrated an extremely high evaporation rate of  $2.6 \text{ kg m}^{-2} \text{ h}^{-1}$  by using a multistage solar still in a rooftop test. That was almost equal to what was produced by the conventional one in the one-day duration of time. The low cost and free of salt accumulation design possibly addressed the practical issues such as long-term operation, salt rejection, and effectual water collection. In addition, the vertically aligned layers and tilt angle provide movement to the device according to the direction and position of the Sun. Even though the device architecture fulfills the earlier requirement of the real-life challenge, the attitude towards high-salinity water and complex fabrication would make it much less competitive in the future market. In this respect, latent heat recovery, scalability, and low design cost should be highly considered when designing the device for larger-scale production (Fig. 16(I)).<sup>206</sup> Because of these, Xue *et al.* proposed a compact solar-thermal membrane distillation system with localized heating, effective cooling, and latent heat recovery features. As shown in Fig. 16(II), the two-consecutive solar-thermal evaporation chambers reutilize the heat loss in one as the heat gain in the other, thereby evidencing latent heat recovery with a recycling facility in the system. With this improvised heat management strategy, the water collection rate was found to be  $1.02 \text{ kg m}^{-2} \text{ h}^{-1}$  with a solar efficiency of 72% obtained under one sun illumination.<sup>207</sup> Later, Chiavazzo and his co-workers also demonstrated a similar design but with multiple distillation sub-stations and recorded impressive freshwater production results at a rate of  $3 \text{ L m}^{-2} \text{ h}^{-1}$ , under one sun illumination, as shown in Fig. 16(III).<sup>208</sup>

Furthermore, with greater progress, a suitable combination of photo-electro-thermal effect on an all-graphene hybrid architecture (as shown in Fig. 16(IV)), solar energy can not only be completely absorbed and transferred into heat but also converted into electric power to further heat up the graphene skeleton frame for a significantly increased generation of water vapor. Therefore, even without system adjustment, the unique graphene evaporator achieves a record-high water production rate of  $2.01\text{--}2.61 \text{ kg m}^{-2} \text{ h}^{-1}$  under solar irradiation of  $1 \text{ kW m}^{-2}$ . The graphene evaporators' several square meters would produce enough water each day to supply tens of people, offering a novel approach to developing a quick and scalable solar steam generating system to solve the water problem.<sup>171</sup>

Despite these incredible achievements in developing a close-to-ideal SIWE system, most of the reported outcomes are still on the laboratory scale, in search of more advancement and novelty toward practical implementation on a large scale. In other words, properties such as low cost, large area, mechanical robustness, and environment-friendly nature must be considered and met. Moreover, the differences between the practical implementation of solar water evaporation systems and laboratory measurements should be regarded before implementing these systems for commercial applications in the near future and hence, the challenges that should be studied and addressed for enhanced system functioning and eventually reaching the commoner's household are listed as follows:



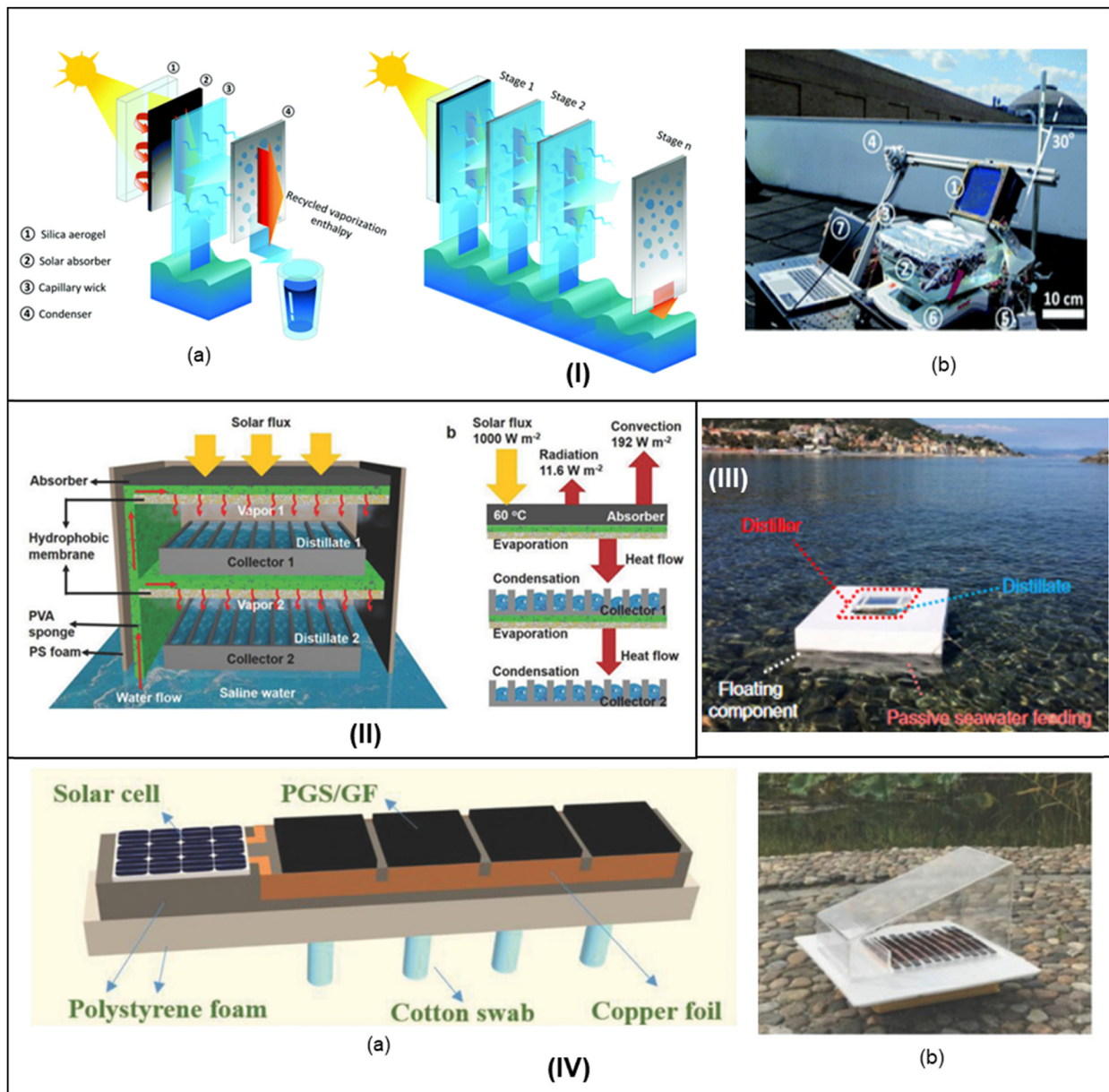


**Fig. 16** (I) Outdoor experiments with the ten-stage TMSS prototype on a partly sunny day with scattered clouds on a rooftop at MIT campus (July 13, 2019). (a) Schematic representation. (b) Experimental setup. Reproduced with permission.<sup>206</sup> Copyright 2020, Royal Society of Chemistry. (II) The multi-level water production device with integrated evaporation and collection design under sun illumination. Reproduced with permission.<sup>207</sup> Copyright 2018, Wiley-VCH. (III) Floating installation of the modular solar distiller. Reproduced with permission.<sup>208</sup> Copyright 2018, Springer Nature. (IV) A hybrid solar-driven PV cell coupled with PGS/GF evaporator. (a) Scheme and (b) figure of the clean water production system based on the pet-PGS/GF arrays working in the outdoor environment. Reproduced with permission.<sup>171</sup> Copyright 2018, Wiley-VCH.

### (i) Synthesis and processing gap of these SIWE devices

Despite the practical material choice, the difficulty and non-relatability of the reported result with large-scale implementation have been an obstacle in this field in the long run. As a result, formulating a uniform and standardized criterion is highly desirable for comparison and evaluations to be made or studied. And hence, an appropriate detailed study of each aspect is necessary to evaluate the parameters and efficiency more effectively, which provides direct feedback for further

exploration of fundamental understanding and practical applications.

### (ii) A reliable and long-term continuous operation

Developing a SIWE system focusing on its ability to function without any interruption for a more extended period with the same capacity and capabilities, in particular, working under natural water sources such as lake water, river water, seawater, industrially contaminated water, city sewage, etc., against



moisture, heat, salt, bacteria, and the erratic weather is a big concern. The current research paid much attention to the enhancement of solar-thermal conversion efficiency and heat management rather than the properties of photoexcitation of the absorber used and the evaporating processes. As a result, the systematic evaluation of the chemical and physical stability of the overall system is still insufficient. Solutions to structural and material engineering, such as chemical/thermal stability, recyclability, surface chemistry, protective coatings, hybridization, and pore structuring, can be perceived.

Other aspects must be avoided, such as fouling, salt clogging, weather incredibility, corrosion, *etc.* For example, the problem of crystallization and precipitation of salts, while working with natural water sources reduces the conversion and evaporation efficiency, respectively. More specifically, the long-term stability and efficiency in brine desalination are the special characteristics of an ideal evaporator. However, despite the fact that numerous scientists have recognized the issue of salt accumulation, it has not been quantified. For example, the amount of salt produced, optimum water concentration, requirement of post-treatment before the operation, and many other parameters. Some factors that play a vital role in salt rejection and simultaneous effective evaporation are the amount of salt rejection per area of evaporating surface, the continuous operation time, the concentration of contaminated water, and the operational interference by different species found in water. Nevertheless, these are the more significant challenges in terms of practical applications and need to be studied and traded off with evaporation efficiency and the proper utilization of solar energy. One more challenge with natural water sources is the contamination of the collected water by volatile organic components and hence, strategizing the structural and material design and separating the volatile organic ingredients from the evaporation process is highly desirable. Before all these, the solar resource's day and night variation obstructs the system's practicality.

### (iii) Output water quality, drinkable or not

Solar interfacial water evaporation has emerged as an efficient, economical, and sustainable desalination method to obtain distilled water. The water obtained through these technologies is claimed to be drinkable and safe. A significant research hole is created when one does not offer the evidence (*i.e.*, the results for the water quality test). For instance, drinking water must be tested for a permissible magnitude for parameters like turbidity, pH, total hardness, calcium, magnesium, copper, iron, manganese, sulfate, chloride, nitrate, fluoride, phenolic compounds, mercury, cadmium, selenium, arsenic, cyanide, lead, zinc, anionic detergents, chromium, mineral oil, and residual free, and also includes color, odor, and taste. Very few compared the salinity magnitude of the feed solution and the distilled water meeting the drinkable water standards against the World Health Organization (WHO)<sup>209</sup> and the US Environmental Protection Agency (EPA).<sup>210</sup> Even few studied the water ion concentration before and after desalination. Hence, the researchers must conduct a rigorous quality comparison before

declaring the water fit for consumption or may be used for other purposes like agriculture. This comparison could subsequently serve as a crucial factor in advancing to practical applications or a real-world scenario, which is the desired next step.

### (iv) To the market, for the people

The overall implementation of the designed system from the laboratory scale to the practical scale is highly inclined towards two key factors, scalability and cost. The fabrication of a novel SIWE device, increasing the solar utilization efficiency, costs more. Other than the price perspective, these advanced designed materials and the development of complex fabrication can hamper the solar water interfacial evaporation on a broader scale. Thus, large-scale manufacturing, simple design, petite structure, and low cost are highly required and advantageous from the product point of view. Generally, regardless of being excellent in other factors, the researchers failed to present the design concerning these factors, thereby causing difficulty in evaluating the potentiality of the practical implementation of the system.

### (v) Lack of integrated solar evaporation system

Despite investigating the development of an ideal solar absorber, an efficient water collection protocol and the integrated water production system remain challenging. Most reports used the conventional transparent plastic cap, glass, or low-density polyethylene (PE) for collecting the evaporated water without considering the collection efficiency and the heat exchange. Other than these, the actual value of evaporation through the set up device can only be determined practically, which would be far different from the observed lab scale, with distinct factors working on it. Moreover, the actual question in water collection, that is, the liquid delivery line, water storage capacity, heat management, energy utilization efficiency, *etc.*, must be thoroughly discussed.

## 5. Conclusions

After a thorough review of the current investigation on the subject, this paper dwells on different aspects of the solar water evaporation system, their purpose and features. Altogether, future development should improve the system performance, from lab to real-life exposure. In other words, a scalable water production system is highly desirable, without external energy usage, for natural and sustainable practical life applications, which can be summarised as a cost-effective and integrated SIWE system, having effectual solar absorption capability, continuous water production, and delivery systems without affecting the natural habitat and surroundings.

Furthermore, considering the remarkable achievements made before, the recommendations for future research can be listed as follows: (i) taking into account the different environmental aspects such as wind, humidity, and temperature in the calculation of the final water evaporation rate or the



conversion efficiency, (ii) minimizing the gap between the current state-of-the-art and practical applications, defining the fabrication and cost involved, (iii) long-term stability of solar-absorber materials on a practical scale with natural water resources, (iv) corrosion, salt accumulation, fouling and other effects of seawater on the functioning surface requires proper understanding along with the recovery mechanism, (v) furthermore, the kinetics including the light and water transport, the ratio of water transport to its evaporation, and the thermal diffusion need to be studied, (vi) a continuous working SIWE device that can operate throughout a day, not during a specific duration, and (vii) lastly, manufacturing and study of these proposed devices, that is, their large scale functioning under diverse applications including water purification, and desalination, electricity generation, sterilization *etc.* Researchers have explored the simultaneous functioning of SIWE devices collectively addressing water, energy, and related environmental issues, but still struggle to meet people's requirements. These pre-described challenges have restricted both the fundamental research and practical examination and hence require an appropriate reasonable solution to produce a clean, green, and sustainable technology.

## Author contributions

All the authors contributed to the manuscript.

## Conflicts of interest

The authors declare no competing financial interest.

## Acknowledgements

The authors are grateful to Director, CSIR-CIMFR, Dhanbad, for his continued support and encouragement.

## References

- 1 H. Sharon and K. S. Reddy, *Renewable Sustainable Energy Rev.*, 2015, **41**, 1080–1118.
- 2 Y. Zhang, M. Sivakumar, S. Yang, K. Enever and M. Ramezanianpour, *Desalination*, 2018, **428**, 116–145.
- 3 T. Arunkumar, K. Raj, D. Dsilva Winfred Rufuss, D. Denkenberger, G. Tingting, L. Xuan and R. Velraj, *Renewable Sustainable Energy Rev.*, 2019, **101**, 197–220.
- 4 H. Ghasemi, G. Ni, A. M. Marconnet, J. Loomis, S. Yerci, N. Miljkovic and G. Chen, *Nat. Commun.*, 2014, **5**, 4449.
- 5 E. T. Ulset, P. Kosinski, Y. Zabednova, O. V. Zhdaneev, P. G. Struchalin and B. V. Balakin, *Nano Energy*, 2018, **50**, 339–346.
- 6 G. Ni, N. Miljkovic, H. Ghasemi, X. Huang, S. V. Boriskina, C.-T. Lin, J. Wang, Y. Xu, M. M. Rahman, T. Zhang and G. Chen, *Nano Energy*, 2015, **17**, 290–301.
- 7 O. Neumann, A. S. Urban, J. Day, S. Lal, P. Nordlander and N. J. Halas, *ACS Nano*, 2013, **7**, 42–49.
- 8 L. Zhou, Y. Tan, J. Wang, W. Xu, Y. Yuan, W. Cai, S. Zhu and J. Zhu, *Nat. Photonics*, 2016, **10**, 393–398.
- 9 P. Zhang, J. Li, L. Lv, Y. Zhao and L. Qu, *ACS Nano*, 2017, **11**, 5087–5093.
- 10 F. Zhao, X. Zhou, Y. Shi, X. Qian, M. Alexander, X. Zhao, S. Mendez, R. Yang, L. Qu and G. Yu, *Nat. Nanotechnol.*, 2018, **13**, 489–495.
- 11 L. Zhu, M. Gao, C. K. N. Peh and G. W. Ho, *Mater. Horiz.*, 2018, **5**, 323–343.
- 12 H. Ren, M. Tang, B. Guan, K. Wang, J. Yang, F. Wang, M. Wang, J. Shan, Z. Chen, D. Wei, H. Peng and Z. Liu, *Adv. Mater.*, 2017, **29**, 1702590.
- 13 H. Bai, T. Zhao and M. Cao, *Mol. Syst. Des. Eng.*, 2020, **5**, 419–432.
- 14 Y. Liu, S. Yu, R. Feng, A. Bernard, Y. Liu, Y. Zhang, H. Duan, W. Shang, P. Tao, C. Song and T. Deng, *Adv. Mater.*, 2015, **27**, 2768–2774.
- 15 Z. Hua, B. Li, L. Li, X. Yin, K. Chen and W. Wang, *J. Phys. Chem. C*, 2017, **121**, 60–69.
- 16 R. Chen, Z. Wu, T. Zhang, T. Yu and M. Ye, *RSC Adv.*, 2017, **7**, 19849–19855.
- 17 X. Zhou, F. Zhao, Y. Guo, Y. Zhang and G. Yu, *Energy Environ. Sci.*, 2018, **11**, 1985–1992.
- 18 F. Yu, Z. Chen, Z. Guo, M. S. Irshad, L. Yu, J. Qian, T. Mei and X. Wang, *ACS Sustainable Chem. Eng.*, 2020, **8**, 7139–7149.
- 19 H. Yang, G. Yang, Z. Qiao, H. Bao, S. Zhang, X. Li and Y. Liu, *ACS Appl. Mater. Interfaces*, 2020, **12**, 35193–35200.
- 20 L. Zhao, Q. Yang, W. Guo, H. Liu, T. Ma and F. Qu, *ACS Appl. Mater. Interfaces*, 2019, **11**, 20820–20827.
- 21 H. Huang, L. Zhao, Q. Yu, P. Lin, J. Xu, X. Yin, S. Chen, H. Wang and L. Wang, *ACS Appl. Mater. Interfaces*, 2020, **12**, 11204–11213.
- 22 X. Chen, C. Meng, Y. Wang, Q. Zhao, Y. Li, X.-M. Chen, D. Yang, Y. Li and Y. Zhou, *ACS Sustainable Chem. Eng.*, 2020, **8**, 1095–1101.
- 23 J. Chen, D. Wang, X. Li, H. Sun, H. Zhao, Y. Li, X. Liu and G. Shi, *ACS Appl. Polym. Mater.*, 2021, **3**, 2402–2410.
- 24 H. Jiang, L. Ai, M. Chen and J. Jiang, *ACS Sustainable Chem. Eng.*, 2020, **8**, 10833–10841.
- 25 S. Tian, Z. Huang, J. Tan, X. Cui, Y. Xiao, Y. Wan, X. Li, Q. Zhao, S. Li and C.-S. Lee, *ACS Energy Lett.*, 2020, **5**, 2698–2705.
- 26 N. S. Lewis, *Science*, 2016, **351**, aad1920.
- 27 J. Liang, H. Liu, J. Yu, L. Zhou and P. Jia, *Nanophotonics*, 2019, **8**, 771–786.
- 28 S. Ishii, R. P. Sugavaneshwar and T. Nagao, *J. Phys. Chem. C*, 2016, **120**, 2343–2348.
- 29 U. Guler, V. M. Shalaev and A. Boltasseva, *Mater. Today*, 2015, **18**, 227–237.
- 30 C. Chang, C. Yang, Y. Liu, P. Tao, C. Song, W. Shang, J. Wu and T. Deng, *ACS Appl. Mater. Interfaces*, 2016, **8**, 23412–23418.
- 31 J. Yang, Y. Chen, X. Jia, Y. Li, S. Wang and H. Song, *ACS Appl. Mater. Interfaces*, 2020, **12**, 47029–47037.



32 P. Qiao, J. Wu, H. Li, Y. Xu, L. Ren, K. Lin and W. Zhou, *ACS Appl. Mater. Interfaces*, 2019, **11**, 7066–7073.

33 A. Kuzmenko, E. Heumen, F. Carbone and D. Marel, *Phys. Rev. Lett.*, 2008, **100**, 117401.

34 Y. Yang, R. Zhao, T. Zhang, K. Zhao, P. Xiao, Y. Ma, P. M. Ajayan, G. Shi and Y. Chen, *ACS Nano*, 2018, **12**, 829–835.

35 Q. Yang, C. Xu, F. Wang, Z. Ling, Z. Zhang and X. Fang, *ACS Appl. Energy Mater.*, 2019, **2**, 7223–7232.

36 Z.-C. Xiong, Y.-J. Zhu, D.-D. Qin and R.-L. Yang, *ACS Appl. Mater. Interfaces*, 2020, **12**, 32556–32565.

37 C.-S. Hu, H.-J. Li, J.-Y. Wang, A. Haleem, X.-C. Li, M. Siddiq and W.-D. He, *ACS Appl. Energy Mater.*, 2019, **2**, 7554–7563.

38 B. Zhu, H. Kou, Z. Liu, Z. Wang, D. K. Macharia, M. Zhu, B. Wu, X. Liu and Z. Chen, *ACS Appl. Mater. Interfaces*, 2019, **11**, 35005–35014.

39 S. Singh, N. Shauloff and R. Jelinek, *ACS Sustainable Chem. Eng.*, 2019, **7**, 13186–13194.

40 C. Xiao, W. Liang, Q.-M. Hasi, F. Wang, L. Chen, J. He, F. Liu, H. Sun, Z. Zhu and A. Li, *ACS Appl. Energy Mater.*, 2020, **3**, 11350–11358.

41 S. Wang, S. M. Almenabawy, N. P. Kherani, S. N. Leung and P. G. O'Brien, *ACS Appl. Energy Mater.*, 2020, **3**, 3378–3386.

42 P. Sun, W. Zhang, I. Zada, Y. Zhang, J. Gu, Q. Liu, H. Su, D. Pantelić, B. Jelenković and D. Zhang, *ACS Appl. Mater. Interfaces*, 2020, **12**, 2171–2179.

43 G. Xue, K. Liu, Q. Chen, P. Yang, J. Li, T. Ding, J. Duan, B. Qi and J. Zhou, *ACS Appl. Mater. Interfaces*, 2017, **9**, 15052–15057.

44 Z. Chen, Q. Li and X. Chen, *ACS Sustainable Chem. Eng.*, 2020, **8**, 13850–13858.

45 M. Ye, J. Jia, Z. Wu, C. Qian, R. Chen, P. G. O'Brien, W. Sun, Y. Dong and G. A. Ozin, *Adv. Energy Mater.*, 2017, **7**, 1–7.

46 X. Liu, H. Cheng, Z. Guo, Q. Zhan, J. Qian and X. Wang, *ACS Appl. Mater. Interfaces*, 2018, **10**, 39661–39669.

47 R. Li, L. Zhang, L. Shi and P. Wang, *ACS Nano*, 2017, **11**, 3752–3759.

48 X. Zhang, G. Wu and X.-C. Yang, *ACS Appl. Nano Mater.*, 2020, **3**, 9706–9714.

49 X. Li, Z. Yao, J. Wang, D. Li, K. Yu and Z. Jiang, *ACS Appl. Energy Mater.*, 2019, **2**, 5154–5161.

50 M. Gao, L. Zhu, C. K. Peh and G. W. Ho, *Energy Environ. Sci.*, 2019, **12**, 841–864.

51 L. Shi, Y. Shi, S. Zhuo, C. Zhang, Y. Aldrees, S. Aleid and P. Wang, *Nano Energy*, 2019, **60**, 222–230.

52 Y. Shi, R. Li, Y. Jin, S. Zhuo, L. Shi, J. Chang, S. Hong, K.-C. Ng and P. Wang, *Joule*, 2018, **2**, 1171–1186.

53 J. Wang, Y. Li, L. Deng, N. Wei, Y. Weng, S. Dong, D. Qi, J. Qiu, X. Chen and T. Wu, *Adv. Mater.*, 2017, **29**, 1603730.

54 S. Cui, H. Liu, L. Gan, Y. Li and D. Zhu, *Adv. Mater.*, 2008, **20**, 2918–2925.

55 L. Xu, L. Cheng, C. Wang, R. Peng and Z. Liu, *Polym. Chem.*, 2014, **5**, 1573–1580.

56 C. Chen, Y. Kuang and L. Hu, *Joule*, 2019, **3**, 683–718.

57 Y. Shi, M. Wang, C. Ma, Y. Wang, X. Li and G. Yu, *Nano Lett.*, 2015, **15**, 6276–6281.

58 G. L. Gibson, T. M. McCormick and D. S. Seferos, *J. Am. Chem. Soc.*, 2012, **134**, 539–547.

59 F. Ni, P. Xiao, C. Zhang, Y. Liang, J. Gu, L. Zhang and T. Chen, *ACS Appl. Mater. Interfaces*, 2019, **11**, 15498–15506.

60 L. Zhang, B. Tang, J. Wu, R. Li and P. Wang, *Adv. Mater.*, 2015, **27**, 4889–4894.

61 Y. Zhang, X. Yin, B. Yu, X. Wang, Q. Guo and J. Yang, *ACS Appl. Mater. Interfaces*, 2019, **11**, 32559–32568.

62 X. Wu, L. Wu, J. Tan, G. Y. Chen, G. Owens and H. Xu, *J. Mater. Chem. A*, 2018, **6**, 12267–12274.

63 Q. Chen, Z. Pei, Y. Xu, Z. Li, Y. Yang, Y. Wei and Y. Ji, *Chem. Sci.*, 2018, **9**, 623–628.

64 X. Zhou, Y. Guo, F. Zhao and G. Yu, *Acc. Chem. Res.*, 2019, **52**, 3244–3253.

65 H. Geng, Q. Xu, M. Wu, H. Ma, P. Zhang, T. Gao, L. Qu, T. Ma and C. Li, *Nat. Commun.*, 2019, **10**, 1512.

66 Z. Fang, S. Jiao, B. Wang, W. Yin and G. Pang, *Glob. Challenges*, 2019, **3**, 1800085.

67 F. Tao, Y. Zhang, S. Cao, K. Yin, X. Chang, Y. Lei, R. Fan, L. Dong, Y. Yin and X. Chen, *Mater. Today Energy*, 2018, **9**, 285–294.

68 Y. Zhang, H. Yan, X. Wang, Z. Zhang, F. Liu, S. Tu and X. Chen, *RSC Adv.*, 2022, **12**, 28997–29002.

69 J. Li, Y. Cui, H. Xiu, W. Wang, M. Du, X. Yang, Q. Xu, E. Kozliak and Y. Ji, *Cellulose*, 2022, **29**, 2461–2477.

70 R. T. Ginting, H. Abdullah, E. Taer, O. Purba and D. Perangin-angin, *Colloids Surf. A*, 2022, **642**, 128653.

71 L. Zhao, P. Wang, J. Tian, J. Wang, L. Li, L. Xu, Y. Wang, X. Fei and Y. Li, *Sci. Total Environ.*, 2019, **668**, 153–160.

72 Y. E. Kim, J. Lim, H. Lee, E. Lee, D. Y. Kim, Y.-S. Jun, J. H. Han and S. H. Lee, *Chemosphere*, 2022, **291**, 133013.

73 F. Cao, K. McEnaney, G. Chen and Z. Ren, *Energy Environ. Sci.*, 2014, **7**, 1615–1627.

74 Q. Jiang, L. Tian, K.-K. Liu, S. Tadepalli, R. Raliya, P. Biswas, R. R. Naik and S. Singamaneni, *Adv. Mater.*, 2016, **28**, 9400–9407.

75 F. Jiang, H. Liu, Y. Li, Y. Kuang, X. Xu, C. Chen, H. Huang, C. Jia, X. Zhao, E. Hitz, Y. Zhou, R. Yang, L. Cui and L. Hu, *ACS Appl. Mater. Interfaces*, 2018, **10**, 1104–1112.

76 Y. Li, T. Gao, Z. Yang, C. Chen, Y. Kuang, J. Song, C. Jia, E. M. Hitz, B. Yang and L. Hu, *Nano Energy*, 2017, **41**, 201–209.

77 F. S. Awad, H. D. Kiriarachchi, K. M. AbouZeid, Ü. Özgür and M. S. El-Shall, *ACS Appl. Energy Mater.*, 2018, **1**, 976–985.

78 X. Hu, W. Xu, L. Zhou, Y. Tan, Y. Wang, S. Zhu and J. Zhu, *Adv. Mater.*, 2017, **29**, 1604031.

79 Z. Yin, H. Wang, M. Jian, Y. Li, K. Xia, M. Zhang, C. Wang, Q. Wang, M. Ma, Q. Zheng and Y. Zhang, *ACS Appl. Mater. Interfaces*, 2017, **9**, 28596–28603.

80 L. Wu, Z. Dong, Z. Cai, T. Ganapathy, N. X. Fang, C. Li, C. Yu, Y. Zhang and Y. Song, *Nat. Commun.*, 2020, **11**, 521.

81 H. Liu, C. Chen, G. Chen, Y. Kuang, X. Zhao, J. Song, C. Jia, X. Xu, E. Hitz, H. Xie, S. Wang, F. Jiang, T. Li, Y. Li, A. Gong, R. Yang, S. Das and L. Hu, *Adv. Energy Mater.*, 2018, **8**, 1701616.



82 M. Zhu, Y. Li, F. Chen, X. Zhu, J. Dai, Y. Li, Z. Yang, X. Yan, J. Song, Y. Wang, E. Hitz, W. Luo, M. Lu, B. Yang and L. Hu, *Adv. Energy Mater.*, 2018, **8**, 1701028.

83 Y. Yang, Y. Sui, Z. Cai and B. Xu, *Glob. Challenges*, 2019, **3**, 1900004.

84 H. M. Wilson, A. R. Shakeelur Rahman, A. E. Parab and N. Jha, *Desalination*, 2019, **456**, 85–96.

85 H. Wilson, A. R. Shakeelur Rahman, R. R. Devarapalli, M. Shelke and N. Jha, *Sol. Energy*, 2018, **159**, 800–810.

86 B. K. Tudu, V. Gupta, A. Kumar and A. Sinhamahapatra, *J. Colloid Interface Sci.*, 2020, **566**, 183–193.

87 L. Zhou, Y. Tan, D. Ji, B. Zhu, P. Zhang, J. Xu, Q. Gan, Z. Yu and J. Zhu, *Sci. Adv.*, 2022, **2**, e1501227.

88 W. Li, Z. Li, K. Bertelsmann and D. E. Fan, *Adv. Mater.*, 2019, **31**, 1900720.

89 X. Wang, Q. Liu, S. Wu, B. Xu and H. Xu, *Adv. Mater.*, 2019, **31**, 1807716.

90 M. Liu, X. Yin, E. Ulin-Avila, B. Geng, T. Zentgraf, L. Ju, F. Wang and X. Zhang, *Nature*, 2011, **474**, 64–67.

91 F. Zhao, Y. Guo, X. Zhou, W. Shi and G. Yu, *Nat. Rev. Mater.*, 2020, **5**, 388–401.

92 Y. Zeng, J. Yao, B. A. Horri, K. Wang, Y. Wu, D. Li and H. Wang, *Energy Environ. Sci.*, 2011, **4**, 4074–4078.

93 Y. Pang, J. Zhang, R. Ma, Z. Qu, E. Lee and T. Luo, *ACS Energy Lett.*, 2020, **5**, 437–456.

94 Z. Xie, Y. Duo, Z. Lin, T. Fan, C. Xing, L. Yu, R. Wang, M. Qiu, Y. Zhang, Y. Zhao, X. Yan and H. Zhang, *Adv. Sci.*, 2020, **7**, 1902236.

95 G. Ni, G. Li, S. V. Boriskina, H. Li, W. Yang, T. J. Zhang and G. Chen, *Nat. Energy*, 2016, **1**, 1–7.

96 L. Shi, X. Wang, Y. Hu, Y. He and Y. Yan, *Appl. Therm. Eng.*, 2020, **179**, 115691.

97 X. Li, G. Ni, T. Cooper, N. Xu, J. Li, L. Zhou, X. Hu, B. Zhu, P. Yao and J. Zhu, *Joule*, 2019, **3**, 1798–1803.

98 N. Xu, X. Hu, W. Xu, X. Li, L. Zhou, S. Zhu and J. Zhu, *Adv. Mater.*, 2017, **29**, 1606762.

99 G. Liu, T. Chen, J. Xu, G. Li and K. Wang, *J. Mater. Chem. A*, 2020, **8**, 513–531.

100 X. Li, W. Xu, M. Tang, L. Zhou, B. Zhu, S. Zhu and J. Zhu, *Proc. Natl. Acad. Sci. U. S. A.*, 2016, **113**, 13953–13958.

101 Y. Ito, Y. Tanabe, J. Han, T. Fujita, K. Tanigaki and M. Chen, *Adv. Mater.*, 2015, **27**, 4302–4307.

102 Y. Liu, J. Chen, D. Guo, M. Cao and L. Jiang, *ACS Appl. Mater. Interfaces*, 2015, **7**, 13645–13652.

103 W. Xu, X. Hu, S. Zhuang, Y. Wang, X. Li, L. Zhou, S. Zhu and J. Zhu, *Adv. Energy Mater.*, 2018, **8**, 1702884.

104 S. Gao, X. Dong, J. Huang, J. Dong, F. Di Maggio, S. Wang, F. Guo, T. Zhu, Z. Chen and Y. Lai, *Glob. Challenges*, 2019, **3**, 1800117.

105 Y. Guo, F. Zhao, X. Zhou, Z. Chen and G. Yu, *Nano Lett.*, 2019, **19**, 2530–2536.

106 Y. Wang, C. Wang, X. Song, M. Huang, S. K. Megarajan, S. F. Shaukat and H. Jiang, *J. Mater. Chem. A*, 2018, **6**, 9874–9881.

107 P. Zhang, Q. Liao, H. Yao, H. Cheng, Y. Huang, C. Yang, L. Jiang and L. Qu, *J. Mater. Chem. A*, 2018, **6**, 15303–15309.

108 V. Kashyap, A. Al-Bayati, S. M. Sajadi, P. Irajizad, S. H. Wang and H. Ghasemi, *J. Mater. Chem. A*, 2017, **5**, 15227–15234.

109 Y. Xia, Q. Hou, H. Jubaer, Y. Li, Y. Kang, S. Yuan, H. Liu, M. Woo, L. Zhang, L. Gao, H. Wang and X. Zhang, *Energy Environ. Sci.*, 2019, **12**, 1840–1847.

110 Y. Xia, Y. Kang, Z. Wang, S. Yuan, Y. Li, L. Gao, H. Wang and X. Zhang, *J. Mater. Chem. A*, 2021, **9**, 6612–6633.

111 O. K. Varghese, M. Paulose, T. J. LaTempa and C. A. Grimes, *Nano Lett.*, 2009, **9**, 731–737.

112 S. Dash, J. de Ruiter and K. K. Varanasi, *Sci. Adv.*, 2022, **4**, eaat0127.

113 Y. Zhang, D. Zhao, F. Yu, C. Yang, J. Lou, Y. Liu, Y. Chen, Z. Wang, P. Tao, W. Shang, J. Wu, C. Song and T. Deng, *Nanoscale*, 2017, **9**, 19384–19389.

114 C. Gong, J. Lao, B. Wang, X. Li, G. Li, J. Gao, Y. Wan, X. Sun, R. Guo and J. Luo, *J. Mater. Chem. A*, 2020, **8**, 20162–20167.

115 X. Li, X. Min, J. Li, N. Xu, P. Zhu, B. Zhu, S. Zhu and J. Zhu, *Joule*, 2018, **2**, 2477–2484.

116 Q. Zhang, L. Li, B. Jiang, H. Zhang, N. He, S. Yang, D. Tang and Y. Song, *ACS Appl. Mater. Interfaces*, 2020, **12**, 28179–28187.

117 E. Traver, R. A. Karaballi, Y. E. Monfared, H. Daurie, G. A. Gagnon and M. Dasog, *ACS Appl. Nano Mater.*, 2020, **3**, 2787–2794.

118 C. Li, D. Jiang, B. Huo, M. Ding, C. Huang, D. Jia, H. Li, C.-Y. Liu and J. Liu, *Nano Energy*, 2019, **60**, 841–849.

119 X. Dong, S. Gao, L. Shuhui, T. Zhu, J. Huang, Z. Chen and Y. Lai, *Mater. Chem. Front.*, 2021, **5**, 1510–1524.

120 J. Li, X. Zhou, P. Mu, F. Wang, H. Sun, Z. Zhu, J. Zhang, W. Li and A. Li, *ACS Appl. Mater. Interfaces*, 2020, **12**, 798–806.

121 J. He, Z. Zhang, C. Xiao, F. Liu, H. Sun, Z. Zhu, W. Liang and A. Li, *ACS Appl. Mater. Interfaces*, 2020, **12**, 16308–16318.

122 D. Hao, Y. Yang, B. Xu and Z. Cai, *Appl. Therm. Eng.*, 2018, **141**, 406–412.

123 M. Y. Wong, Y. Zhu, T. C. Ho, A. Pan and C. Y. Tso, *Appl. Therm. Eng.*, 2023, **219**, 119686.

124 X. Gao, H. Lan, S. Li, X. Lu, M. Zeng, X. Gao, Q. Wang, G. Zhou, J.-M. Liu, M. J. Naughton, K. Kempa and J. Gao, *Glob. Challenges*, 2018, **2**, 1800035.

125 P. Ying, M. Li, F. Yu, Y. Geng, L. Zhang, J. He, Y. Zheng and R. Chen, *ACS Appl. Mater. Interfaces*, 2020, **12**, 32880–32887.

126 C. Xue, S. Hu, Q. Chang, N. Li, Y. Wang, W. Liu and J. Yang, *J. Mater. Sci.*, 2018, **53**, 9742–9754.

127 S. Namboorimadathil Backer, A. M. Ramachandran, A. A. Venugopal, A. P. Mohamed, A. Asok and S. Pillai, *ACS Appl. Nano Mater.*, 2020, **3**, 6827–6835.

128 B. Yuan, L. Meng, C. Zhang, L. Yang, L. Bai, H. Yang, D. Wei, F. Wang, Q. Wang, W. Wang and H. Chen, *Appl. Surf. Sci.*, 2021, **570**, 151143.

129 J. Deng, S. Xiao, B. Wang, Q. Li, G. Li, D. Zhang and H. Li, *ACS Appl. Mater. Interfaces*, 2020, **12**, 51537–51545.



130 Y. Xu, J. Ma, Y. Han, J. Zhang, F. Cui, Y. Zhao, X. Li and W. Wang, *ACS Sustainable Chem. Eng.*, 2019, **7**, 5476–5485.

131 D. Zhang, Y. Cai, Q. Liang, Z. Wu, N. Sheng, M. Zhang, B. Wang and S. Chen, *ACS Sustainable Chem. Eng.*, 2020, **8**, 9017–9026.

132 Q. Hou, C. Xue, N. Li, H. Wang, Q. Chang, H. Liu, J. Yang and S. Hu, *Carbon*, 2019, **149**, 556–563.

133 X. Feng, J. Zhao, D. Sun, L. Shanmugam, J.-K. Kim and J. Yang, *J. Mater. Chem. A*, 2019, **7**, 4400–4407.

134 Y. Wang, C. Wang, X. Song, S. K. Megarajan and H. Jiang, *J. Mater. Chem. A*, 2018, **6**, 963–971.

135 J. Wang, Z. Liu, X. Dong, C.-E. Hsiung, Y. Zhu, L. Liu and Y. Han, *J. Mater. Chem. A*, 2017, **5**, 6860–6865.

136 V. Ovando-Medina, A. G. Escobar Villanueva, H. Martínez Gutiérrez and O. Gonzalez-Ortega, *Int. J. Energy Res.*, 2020, **44**, 10878–10893.

137 H. Wang, C. Zhang, Z. Zhang, B. Zhou, J. Shen and A. Du, *Sol. RRL*, 2021, **5**, 2000817.

138 Q. Qi, Y. Wang, W. Wang, X. Ding and D. Yu, *Sci. Total Environ.*, 2020, **698**, 134136.

139 F. Liu, L. Wang, R. Bradley, B. Zhao and W. Wu, *Adv. Sustainable Syst.*, 2020, **4**, 1900122.

140 H. Xiong, X. Xie, M. Wang, Y. Hou and X. Hou, *Acta Phys.-Chim. Sin.*, 2020, **36**, 1912008.

141 Y. Xia, Y. Li, S. Yuan, Y. Kang, M. Jian, Q. Hou, L. Gao, H. Wang and X. Zhang, *J. Mater. Chem. A*, 2020, **8**, 16212–16217.

142 N. Xu, J. Li, Y. Wang, C. Fang, X. Li, Y. Wang, L. Zhou, B. Zhu, Z. Wu, S. Zhu and J. Zhu, *Sci. Adv.*, 2022, **5**, eaaw7013.

143 Y. Li, T. Gao, Z. Yang, C. Chen, W. Luo, J. Song, E. Hitz, C. Jia, Y. Zhou, B. Liu, B. Yang and L. Hu, *Adv. Mater.*, 2017, **29**, 1700981.

144 L. Zhao, C. Du, C. Zhou, S. Sun, Y. Jia, J. Yuan, G. Song, X. Zhou, Q. Zhao and S. Yang, *ACS Sustainable Chem. Eng.*, 2020, **8**, 4362–4370.

145 Q. Fang, T. Li, H. Lin, R. Jiang and F. Liu, *ACS Appl. Energy Mater.*, 2019, **2**, 4354–4361.

146 J.-K. Xiao, J.-Z. Gong, M. Dai, Y.-F. Zhang, S.-G. Wang, Z. Lin, D. Feipeng and P. Fu, *J. Alloys Compd.*, 2022, **930**, 167404.

147 G. Zhu, J. Xu, W. Zhao and F. Huang, *ACS Appl. Mater. Interfaces*, 2016, **8**, 31716–31721.

148 W. Zhao, H. Gong, Y. Song, B. Li, N. Xu, X. Min, G. Liu, B. Zhu, L. Zhou, X.-X. Zhang and J. Zhu, *Adv. Funct. Mater.*, 2021, **31**, 2100025.

149 L. Shi, Y. Wang, L. Zhang and P. Wang, *J. Mater. Chem. A*, 2017, **5**, 16212–16219.

150 N. Shahidzadeh-Bonn, S. Rafai, D. Bonn and G. Wegdam, *Langmuir*, 2008, **24**, 8599–8605.

151 Y. Zhang, T. Xiong, D. K. Nandakumar and S. C. Tan, *Adv. Sci.*, 2020, **7**, 1903478.

152 G. Ni, S. H. Zandavi, S. M. Javid, S. V. Boriskina, T. A. Cooper and G. Chen, *Energy Environ. Sci.*, 2018, **11**, 1510–1519.

153 S. Cheng, Z. Yu, Z. Lin, L. Li, Y. Li and Z. Mao, *Chem. Eng. J.*, 2020, **401**, 126108.

154 Y. Yang, H. Zhao, Z. Yin, J. Zhao, X. Yin, N. Li, D. Yin, Y. Li, B. Lei, Y. Du and W. Que, *Mater. Horiz.*, 2018, **5**, 1143–1150.

155 R. Hu, J. Zhang, Y. Kuang, K. Wang, X. Cai, Z. Fang, W. Huang, G. Chen and Z. Wang, *J. Mater. Chem. A*, 2019, **7**, 15333–15340.

156 B. Shao, Y. Wang, X. Wu, Y. Lu, X. Yang, G. Y. Chen, G. Owens and H. Xu, *J. Mater. Chem. A*, 2020, **8**, 11665–11673.

157 S. Han, J. Yang, X. Li, W. Li, X. Zhang, N. Koratkar and Z.-Z. Yu, *ACS Appl. Mater. Interfaces*, 2020, **12**, 13229–13238.

158 C. Shen, Y. Zhu, X. Xiao, X. Xu, X. Chen and G. Xu, *ACS Appl. Mater. Interfaces*, 2020, **12**, 35142–35151.

159 Y. Guo, X. Zhou, F. Zhao, J. Bae, B. Rosenberger and G. Yu, *ACS Nano*, 2019, **13**, 7913–7919.

160 P. Fan, H. Wu, M. Zhong, H. Zhang, B. Bai and G. Jin, *Nanoscale*, 2016, **8**, 14617–14624.

161 S. Hong, Y. Shi, R. Li, C. Zhang, Y. Jin and P. Wang, *ACS Appl. Mater. Interfaces*, 2018, **10**, 28517–28524.

162 P. Xiao, J. He, F. Ni, C. Zhang, Y. Liang, W. Zhou, J. Gu, J. Xia, S.-W. Kuo and T. Chen, *Nano Energy*, 2020, **68**, 104385.

163 L. Zhu, M. Gao, C. K. N. Peh, X. Wang and G. W. Ho, *Adv. Energy Mater.*, 2018, **8**, 1702149.

164 A. Tamburini, M. Tedesco, A. Cipollina, G. Micale, M. Ciofalo, M. Papapetrou, W. Van Baak and A. Piacentino, *Appl. Energy*, 2017, **206**, 1334–1353.

165 S. Lin, N. Y. Yip, T. Y. Cath, C. O. Osuji and M. Elimelech, *Environ. Sci. Technol.*, 2014, **48**, 5306–5313.

166 P. Yang, K. Liu, Q. Chen, J. Li, J. Duan, G. Xue, Z. Xu, W. Xie and J. Zhou, *Energy Environ. Sci.*, 2017, **10**, 1923–1927.

167 L. Zhu, T. Ding, M. Gao, C. K. N. Peh and G. W. Ho, *Adv. Energy Mater.*, 2019, **9**, 1900250.

168 M. Gao, C. Peh, H. Phan, L. Zhu and G. Ho, *Adv. Energy Mater.*, 2018, **8**, 1800711.

169 L. Zong, M. Li and C. Li, *Nano Energy*, 2018, **50**, 308–315.

170 X. Yuan, Z. Li, Y. Shao, D. Yang, K. Hu, H. You, Z. Xu, S. Hua, W. Liu, P. Peng, Y. Yan and X. Tang, *J. Mater. Chem. C*, 2022, **10**, 6456–6463.

171 L. Cui, P. Zhang, Y. Xiao, Y. Liang, H. Liang, Z. Cheng and L. Qu, *Adv. Mater.*, 2018, **30**, 1706805.

172 F. L. Meng, M. Gao, T. Ding, G. Yilmaz, W. L. Ong and G. W. Ho, *Adv. Funct. Mater.*, 2020, **30**, 2002867.

173 X. Peng, H. Jiang, N. Feng, C. Zhang, L. Yun, W. Zhou, J. Gu, J. Xia, S.-W. Kuo and T. Chen, *Nano Energy*, 2019, **68**, 104385.

174 T. Ding and G. W. Ho, *Joule*, 2021, **5**, 1639–1641.

175 Q. Ji, N. Li, S. Wang, S. Li, F. Li, L. Yu, P. Murto and X. Xu, *J. Mater. Chem. A*, 2021, **9**, 21197–21208.

176 Y. Huang, C. Wang, C. Shao, B. Wang, N. Chen, H. Jin, H. Cheng and L. Qu, *Acc. Mater. Res.*, 2021, **2**, 97–107.

177 Z. Sun, C. Han, S. Gao, Z. Li, M. Jing, H. Yu and Z. Wang, *Nat. Commun.*, 2022, **13**, 5077.

178 Y. Xu, J. Wang, F. Yu, Z. Guo, H. Cheng, J. Yin, L. Yan and X. Wang, *ACS Sustainable Chem. Eng.*, 2020, **8**, 12053–12062.

179 C. Chang, P. Tao, J. Xu, B. Fu, C. Song, J. Wu, W. W. Shang and T. Deng, *ACS Appl. Mater. Interfaces*, 2019, **11**, 18466–18474.



180 X. Ma, Z. Deng, Z. Li, D. Chen, X. Wan, X. Wang and X. Peng, *J. Mater. Chem. A*, 2020, **8**, 22728–22735.

181 X. Li, J. Li, J. Lu, N. Xu, C. Chen, X. Min, B. Zhu, H. Li, L. Zhou, S. Zhu, T. Zhang and J. Zhu, *Joule*, 2018, **2**, 1331–1338.

182 J. Li, M. Du, G. Lv, L. Zhou, X. Li, L. Bertoluzzi, C. Liu, S. Zhu and J. Zhu, *Adv. Mater.*, 2018, **30**, 1805159.

183 Z. Zhao, G. Jia, Y. Liu, Q. Zhang, Y. Zhou and K. Chang, *ACS Omega*, 2020, **5**, 13482–13488.

184 W. Li, M. C. Tekell, Y. Huang, K. Bertelsmann, M. Lau and D. Fan, *Adv. Energy Mater.*, 2018, **8**, 1802108.

185 X. Xu, S. Ozden, N. Bizmark, C. B. Arnold, S. S. Datta and R. D. Priestley, *Adv. Mater.*, 2021, **33**, 2007833.

186 D. Qi, Y. Liu, Y. Liu, Z. Liu, Y. Luo, H. Xu, X. Zhou, J. Zhang, H. Yang, W. Wang and X. Chen, *Adv. Mater.*, 2020, **32**, 2004401.

187 C. Chen, L. Zhou, J. Yu, Y. Wang, S. Nie, S. Zhu and J. Zhu, *Nano Energy*, 2018, **51**, 451–456.

188 L. Yang, G. Chen, N. Zhang, Y. Xu and X. Xu, *ACS Sustainable Chem. Eng.*, 2019, **7**, 19311–19320.

189 Y. Guo, H. Lu, F. Zhao, X. Zhou, W. Shi and G. Yu, *Adv. Mater.*, 2020, **32**, 1907061.

190 D. Hao, Y. Yang, B. Xu and Z. Cai, *ACS Sustainable Chem. Eng.*, 2018, **6**, 10789–10797.

191 M.-Q. Yang, C. F. Tan, W. Lu, K. Zeng and G. W. Ho, *Adv. Funct. Mater.*, 2020, **30**, 2004460.

192 Z. Deng, L. Miao, L. Peng-Fei, J. Zhou, P. Wang, Y. Gu, X. Wang, H. Cai, L. Sun and S. Tanemura, *Nano Energy*, 2019, **55**, 368–376.

193 Z. Yu, S. Cheng, C. Li, L. Li and J. Yang, *ACS Appl. Mater. Interfaces*, 2019, **11**, 32038–32045.

194 Z. Wang, P. Guo, L. Heng and L. Jiang, *Matter*, 2021, **4**, 1274–1286.

195 F. Ni, P. Xiao, N. Qiu, C. Zhang, Y. Liang, J. Gu, J. Xia, Z. Zeng, L. Wang, Q. Xue and T. Chen, *Nano Energy*, 2020, **68**, 104311.

196 W. Huang, P. Su, Y. Cao, C. Li, D. Chen, X. Tian, Y.-Q. Su, B. Qiao, J. Tu and X. Wang, *Nano Energy*, 2020, **69**, 104465.

197 O. Neumann, C. Feronti, A. D. Neumann, A. Dong, K. Schell, B. Lu, E. Kim, M. Quinn, S. Thompson, N. Grady, P. Nordlander, M. Oden and N. J. Halas, *Proc. Natl. Acad. Sci. U. S. A.*, 2013, **110**, 11677–11681.

198 M. Gao, P. K. N. Connor and G. W. Ho, *Energy Environ. Sci.*, 2016, **9**, 3151–3160.

199 O. Neumann, A. D. Neumann, S. Tian, C. Thibodeaux, S. Shubhankar, J. Müller, E. Silva, A. Alabastri, S. W. Bishnoi, P. Nordlander and N. J. Halas, *ACS Energy Lett.*, 2017, **2**, 8–13.

200 C. Chang, P. Tao, B. Fu, J. Xu, C. Song, J. Wu, W. Shang and T. Deng, *ACS Omega*, 2019, **4**, 3546–3555.

201 C. Wu, H. Geng, S. Tan, J. Lv, H. Wang, Z. He and J. Wang, *Mater. Horiz.*, 2020, **7**, 2097–2104.

202 T. Cheng, R. He, Q. Zhang, X. Zhan and F. Chen, *J. Mater. Chem. A*, 2015, **3**, 21637–21646.

203 G. Jiang, L. Chen, S. Zhang and H. Huang, *ACS Appl. Mater. Interfaces*, 2018, **10**, 36505–36511.

204 P. Zhang, Q. Liao, T. Zhang, H. Cheng, Y. Huang, C. Yang, C. Li, L. Jiang and L. Qu, *Nano Energy*, 2018, **46**, 415–422.

205 Y. Fan, Z. Tian, F. Wang, J. He, X. Ye, Z. Zhu, H. Sun, W. Liang and A. Li, *ACS Appl. Energy Mater.*, 2021, **4**, 2932–2943.

206 Z. Xu, L. Zhang, L. Zhao, B. Li, B. Bhatia, C. Wang, K. L. Wilke, Y. Song, O. Labban, J. H. Lienhard, R. Wang and E. N. Wang, *Energy Environ. Sci.*, 2020, **13**, 830–839.

207 G. Xue, Q. Chen, S. Lin, J. Duan, P. Yang, K. Liu, J. Li and J. Zhou, *Glob. Challenges*, 2018, **2**, 1800001.

208 E. Chiavazzo, M. Morciano, F. Viglino, M. Fasano and P. Asinari, *Nat. Sustainable*, 2018, **1**, 763–772.

209 *Guidelines for drinking-water quality: Fourth edition incorporating the first and second addenda*, World Health Organisation, Geneva, 2022, ISBN: 978-92-4-004506-4.

210 U.S. EPA National Primary Drinking Water Regulations, 2022.

